Final Report

Project Title: Hot Superplastic Powder Forging for Transparent Nanocrystalline Ceramics
Principal Investigator/Project Director: W. Roger Cannon
Budget Period: 09/01/2002 to 032/28/2006
Recipient Organization: Rutgers, the State University of New Jersey
Office of Research and Sponsored Programs
3 Rutgers Plaza ASB III
DOE Award Number: DE-FG02-02ER46010
Anticipated Funds left at end of program: not significant.

Summary:

The goal of the program was to fabricate nanocrystalline ceramics from superplastically deforming powder with nanocrystalline microstructures using a new approach. Rather than starting with nano-sized powders, we used powders 2-25 μm in diameter (average 16 μm) having a nanoscale microstructure. The major challenge was to hot press or to hot forge the powders to full density while maintaining the nanostructure. The second goal was to achieve transparent nanocrystalline ceramics.

Accomplishments: The first goal of fabricating nanocrystalline ceramics from superplastically deforming powder was accomplished. However, not all features of the microstructure were <100 nm. It was found, for instance, that in the fully dense Al_2O_3-ZrO_2 eutectic specimens that a bicontinuous microstructure exists containing <100 nm ZrO_2 particles in a matrix of Al_2O_3 grains extending over 1-2 μm was observed. Crystallization, growth, phase development and creep during hot pressing and forging were studied for several compositions and so provided some details on development of polycrystalline microstructure from heating quenched ceramics. It was predicted, however, that fully nanostructured microstructures of the Al_2O_3-ZrO_2 composition could not be hot pressed at pressures on the order of 100 MPa. The second goal of transparent nanocrystalline ceramics was not achieved because of microstructure coarsening though thin sections of some samples were translucent.

Education: Mr. Hrishi Keshavan, supported by this program, will complete his Ph.D July 2006. Ms. Chiraporn Auechalitanukul, supported by a Thai government fellowship, but also receiving partial support from this program, will also complete her Ph.D July 2006. Dr Sreeram Balasubramanian, Research Associate, until September 2003, accepted a position with Surmed Inc. Dr. Evgenia Perkaskaya, Research Associate, until May 2004, accepted a position as Director of the Keck Electron Microscopy Laboratory, Polymer Science & Engineering, UMass, Amherst. Dr. Anders Petersson served as postdoctoral fellow from June 2004 through the end of the program.

Research Accomplishments

Introduction. This program studied an alternate and, for some applications improved method of obtaining nanocrystalline ceramics. Typically, nanocrystalline ceramics are fabricated starting with powder of particle diameter on the order of a ten nanometers, with the intent of maintaining that diameter through pressureless sintering, hot pressing or hot forging. Several disadvantages of this method are: (1) Powders are difficult to handle and difficult to avoid agglomeration during the forming operation. (2) Powders, in dry forming operations, hydrate or pick up other impurities because of their high specific surface area. (3) Adsorbed gases, water vapor from hydration and

other gases are trapped during sintering are difficult to eliminate from a powder compact and limit the final density. (4) Inhalation of nano-particulate powders may pose a health hazard.

As an alternative, this program studied coarse spherical powders (<25 μm in diameter and average 16 μm) rapidly quenched from the melt, whose microstructure ranged from fully nanocrystalline to fully amorphous. The program, however, mostly concentrated on the Al_2O_3-ZrO_2 eutectic powders, which after quenching from the melt were between 30% and 40% amorphous. These powders were then hot pressed and forged to study their densification behavior.

Two important aspects of the program were, first, a study of microstructure development from the as-quenched state to various annealing temperatures and then through the hot pressing stage and, second, the kinetics of hot pressing and hot forging. These two aspects of the technology are summarized in two papers attached to this report [1,2,3]

Several contributions of the program were: (1) This program presented a detailed description of microstructural development during hot pressing of multigrain powders. Only a few previous studies have hot pressed multigrain powder [4,5,6,7] but did not provide a thorough discussion of the microstructure. Furthermore, little discussion has been devoted to microstructure development of melt quenched powders. (2) The program presented the first model study of kinetics of hot pressing of spherical multigrained powders densifying by creep. Although Ashby and colleagues had previously presented simplified models for predicting densification rates by creep, no previous study had compared experimental studies on densification of idealized uniform spherical particles with the simple models. In addition a somewhat more complex finite element model was developed.[1] (3) The kinetics of hot pressing of the unique microstructure that developed from the quenched powders was determined. (4) Methods for hot pressing in air using alumina and silicon carbide dies and for extrusion in silicon carbide dies were developed. Each of the aspects of this program are summarized below. A more thorough discussion is contained in the two unpublished papers attached to this report.

Table I Chemical compositions in mass % (vol.%)

Composition	Alumina	Zirconia	Magnesium aluminate spinel	Boro-silicate glass	Theoretical densities (g/cm^3)
AZY	57.8(67.3)	42.2 (32.6)[a]	-	-	4.7
AZ	57.8(67.3)	42.2(32.6)	-	-	4.7
AZYG	57.8(62.5)	42.2(30.2) [a]	-	4.0(7.2)	4.6
SZY	-	36.9(25.9) [a]	63.1(73.9)	-	4.1
SZYG	-	36.9(24.2) [a]	63.1(69.1)	4.0(6.57)	4.2
AZSY	25.2(29.6)	49.9(38.4)	24.9(31.9)	-	4.9

[a] stabilized with 1 mol % yttria

Microstructural Development. Microstructural development of several different eutectic compositions was studied in this program (see Table I) but the most thorough study was of the AZY composition. These results are reported below. Some details of microstructural development are reported in paper I of the appendix.

In appearance the spherical as-quenched particles were smooth and transparent. By analysis of the amorphous broad x-ray peak at low angles, it was determined that particles were between 30% and 40% amorphous. TEM analysis, supported by x-ray analysis, indicated that the remaining 60% to 70% contained γ-Al_2O_3 and t-ZrO_2 crystallites between 20 and 50 nm in diameter. (Fig. 1 (a)) The SAD pattern clearly showed a polycrystalline spotted ring, as well as the amorphous ring. These micrographs were taken by thinning particles embedded in epoxy.

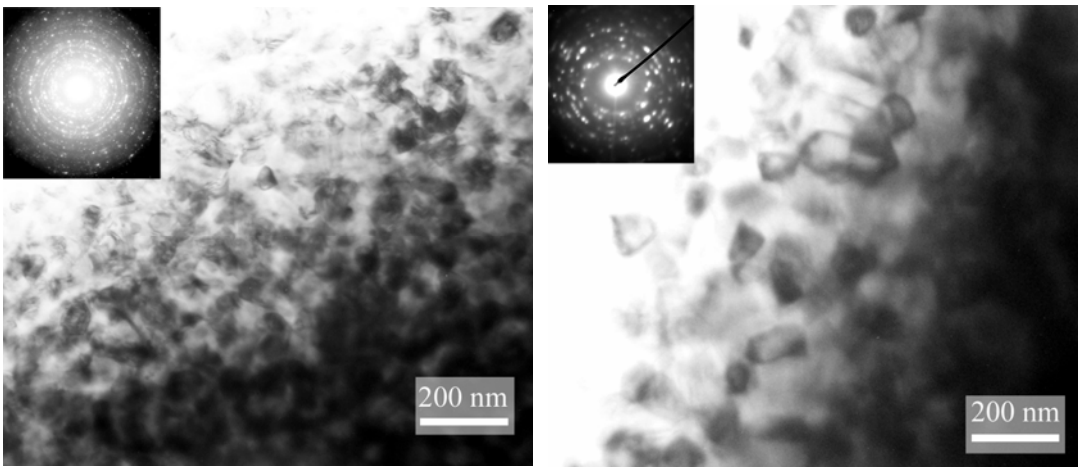

(a) (b)

Figure 1. Bright field TEM images and SAD of (a) as-quenched and (b) 1250ºC, 4 hr annealed AZY powder. Light phase is alumina and dark phase is zirconia.

Microstructural changes during heating were determined by annealing studies at various temperatures and by DTA scans to monitor crystallization. A strong exothermic peak was observed at 959ºC. This peak changed the Al_2O_3:ZrO_2 from 1.1:1 in the as-quenched powder, to (0.7-0.8):1 indicating that more amorphous ZrO_2 crystallized at this temperature than Al_2O_3. A small amount of amorphous material, mainly Al_2O_3 crystallized at still higher temperatures. By 1150ºC the two phase microstructure was visible by secondary electron scattering in SEM. Both phases were in the nano-size range and the microstructure had a vermicular appearance. At 1250ºC the crystallites had coarsened very little (Fig. 2(b)). Annealing at temperatures between 1250ºC and 1350º coarsened the microstructure. Coarsening occurred more rapidly under deformation conditions during hot pressing or hot forging.

Specimens were first hot pressed from the as-quenched powder in air at 1250ºC. Then porous specimens were removed from the die and hot forged at either 1250 or 1350ºC. Hot pressed or hot forged microstructures were always coarser than the microstructures of particles annealed without pressure for the same time/temperature cycle, indicating some sort of dynamic coarsening. The microstructure was rather complex and could not be described by a single grain size or even by the particle diameter of each phase. The most uniformly consistent structure was 50-100 nm ZrO_2 particles (perhaps interconnected in 3D over a short distance) spread throughout the microstructure. Understanding of the matrix Al_2O_3 (67 vol.%) phase was enhanced by viewing the pair of bright field and dark field images shown in Figs. 2(a) and 2(b), taken from a 1350ºC hot forged specimen. Examination of Fig. 2(b) reveals that Al_2O_3 is bright over much of the micrograph (1.25 μm wide x 1.5 μm high) indicating a common crystallographic orientation but there are dark regions of Al_2O_3 indicating a different crystallographic orientation. Thus the rmicrograph covers at least two intertwined Al_2O_3 grains. The apparently gerrymandered shape of the grain possibly is to minimize the Al_2O_3-Al_2O_3 boundary area since Al_2O_3-ZrO_2 boundaries are lower energy.

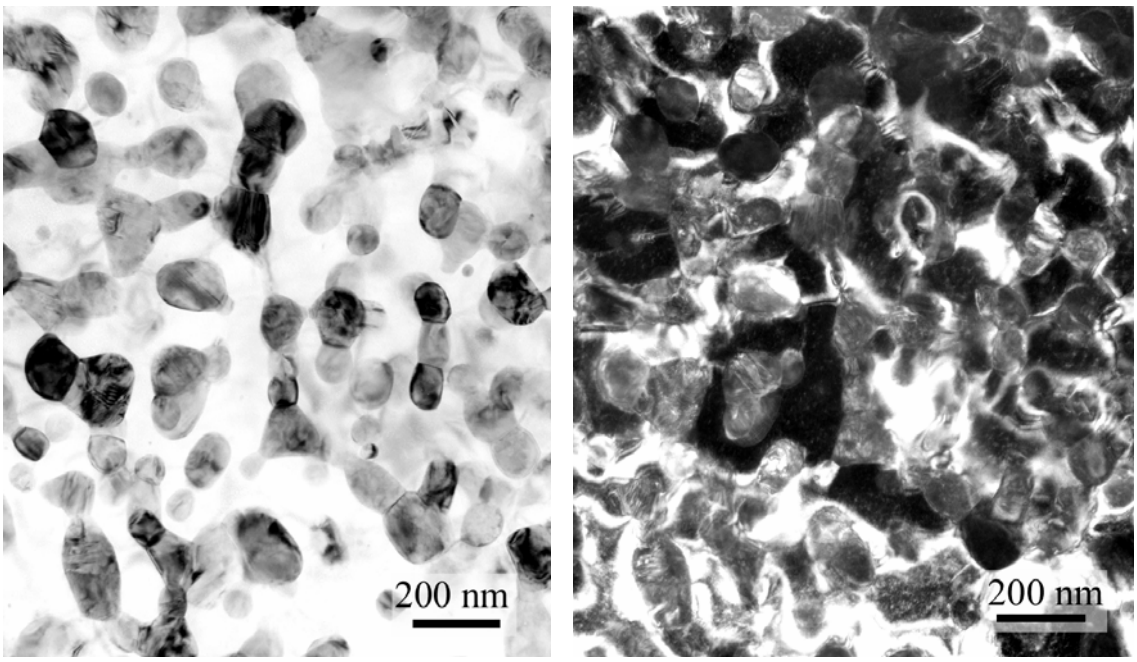

(a) (b)

Figure 2. TEM micrographs of quenched AZY after forging at 1350ºC. (a) ZrO_2 is dark and Al_2O_3 is light in bright field. (b) In dark field the brightest portions come from one Al_2O_3 diffraction spot. The aperture may also have covered a ZrO_2 spot.

At a lower magnification there is a second characteristic microstructure shown in Fig. 3, generally observed in most regions of the specimens. There are approximately 2 μm diameter areas of the micrograph whose perimeters are decorated with ZrO_2 stringers. We have designated these as cells. These were originally thought to be the extent of a continuous grain of Al_2O_3 but according to Fig. 2(b) a number of crystals of Al_2O_3 are intertwined within each of these cells. At present we believe these to be high angle grain boundaries formed as growing crystals from adjacent cells meet, perhaps leaving some amorphous material along the boundary. During deformation these boundaries shear creating high angle boudaries. ZrO_2 decorates the boundary to minimize interface energy. Chen and Xue[8] examined a large number of dihedral angles in Al_2O_3-ZrO_2 composites and concluded that the interface energy followed the order $\gamma_{Al_2O_3-Al_2O_3} > \gamma_{Al_2O_3-tZrO_2} > \gamma_{tZrO_2-tZrO_2}$. Interface energy is reduced if ZrO_2 particles migrate to the boundary. The evidence for this is that zones denuded of ZrO2 often surround the boundaries. Since this structure develops much more rapidly under strain than in static conditions, it is

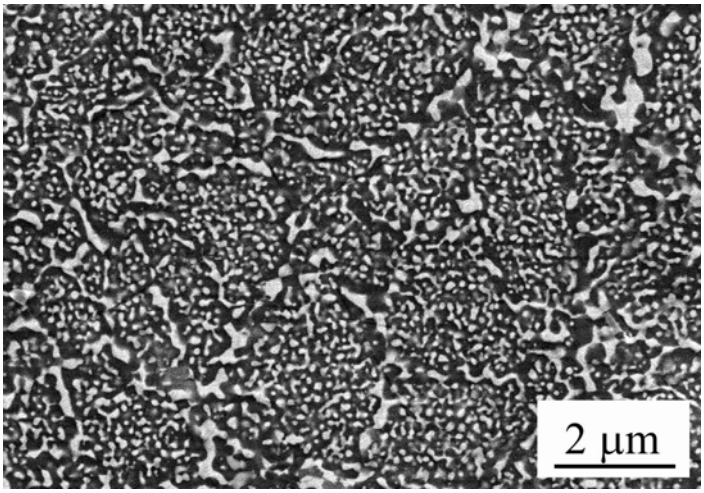

Figure 3. SEM micrograph of Al_2O_3-(1Y)ZrO_2 forged at 1350 °C for 1 h at ~50 MPa. Al_2O_3 is dark phase and ZrO_2 is light phase.

suggested that these boundaries are boundaries of shear.

In the accompanying paper the microstructures of the other compositions listed in Table I are described. The microstructures have many similar features leading to the conclusion that these features are common for hot pressed or hot forged particles quenched from the melt.

Kinetics. Considering the complex microstructure, kinetics of densification are also somewhat more difficult to describe. When the microstructural features are much smaller than the particle size which is the case here, densification is controlled by particle creep. Nabarro-Herring, Coble or superplastic creep are all possible creep mechanisms. Each is dependent on grain size. When the grain size is much smaller than the particle size, the controlling diffusion distance is the grain diameter rather than the length of the interparticle neck. The roll of the grain boundary in these mechanisms is to act as a source or sink of vacancies (Nabarro-Herring, Coble), as a diffusion path (Coble) or as a plane of shear. Since it was not clearly evident which boundaries might fulfill these functions, densification kinetics were measured and then the mechanism of densification and microstructural contributions were determined.

Although HIPping might accomplish full densification at a high temperature and pressure, it was not possible to perform at our university and it lacks the ability to measure kinetics. Two types of studies were performed in an air atmosphere. First, small cylindrical specimens were hot pressed in throw-way alumina dies to a density less than 80% of theoretical. The specimens were then removed and forged without a die. The reason for this was that high densities (rarely >80%) could not be reached by hot pressing in a die whereas rapid densification to near theoretical density could be reached for all specimens by hot forging. The kinetics were routinely measured only during forging. In the second set of experiments, the kinetics of hot pressing in a silicon carbide dies were studied to compare experimental rates with rates predicted by equations for hot pressing and HIPping. Also a temperature dependence study of densification rates was performed on specimens in alumina dies.

In order to estimate the creep rate of the quenched spherical particles, which are fully dense, the strain rate for the last 5 minutes of forging was used with a correction for porosity, by multiplying the creep rate by the factor k_p [9]

$$k_p = \frac{\left\{1+\beta P \Big/ \left[1-(\beta+1)P\right]\right\}^{1-n}}{\left(1-P^{2/3}\right)^n} \qquad (1)$$

where β=*-4* and P is the fraction of porosity. From the creep results the stress and temperature dependence could be derived.

Fig. 4 contains a summary of creep rates measured at 1250C and 1350ºC. It indicates that creep rates, and therefore, expected densification rates, were most rapid for the $MgAl_2O_4$ spinel containing compositions and that borosilicate glass additives enhanced the creep rates of other compositions. Typical stress exponents were *n=1.5* , indicating a diffusional creep mechanism.

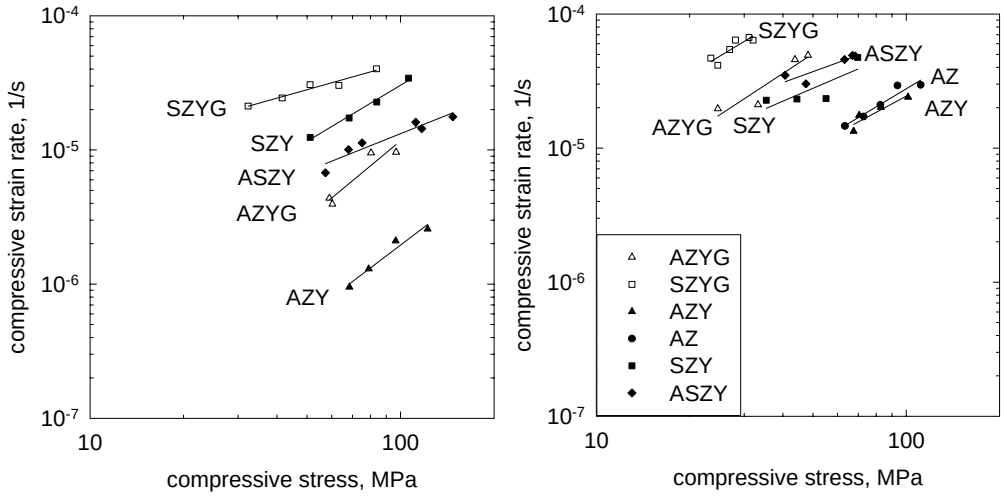

Figure 4. Strain rates determined after 60 min sinter-forging at (a) 1250ºC and (b) 1350ºC.

The temperature dependence is more complex and rather unusual. The tests were performed in such a way that the specimens had not experienced a higher temperature than the creep test temperature. In order to test densification rates at temperatures <1200ºC, it was necessary to measure creep of powder in a die since hot pressed specimens were too fragile to withstand high stresses. Then the porosity correction was applied. Results are shown in Fig. 5. The important feature was the sudden decrease in creep rates in all curves at temperatures somewhere between 1200 and 1300ºC. Although this was the approximate range for microstructure coarsening, the sudden drop in creep rates with increasing temperature was not a result of rapid coarsening of structure. Microstructures just below the sudden temperature drop were very similar to those just above the temperature drop. An explanation more consistent with experimental results for the AZY and ASZY compositions is that the transformation of γ-Al_2O_3 to α-Al_2O_3 occurs in this temperature range. This explanation, however, does not help understand the break in the curve for the SZY composition, containing no Al_2O_3. A third explanation is that this is the temperature of elimination of the final small fraction of amorphous phase surrounding the cell boundaries and that shearing of and/or diffusion along the cell boundaries limits the creep rates..

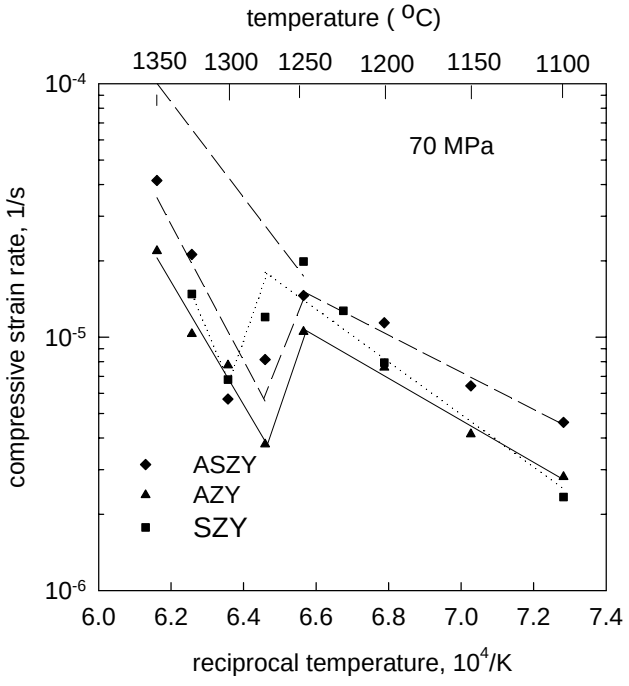

Figure 5. Strain rates determined after 60 min hot pressing at 70 MPa: (▲,—) AZY, (■,···) SZY, (◆,- - -) ASZY, and determined from sinter-forging and compensated for decreasing effective pressure: (◇,- - -) ASZY.

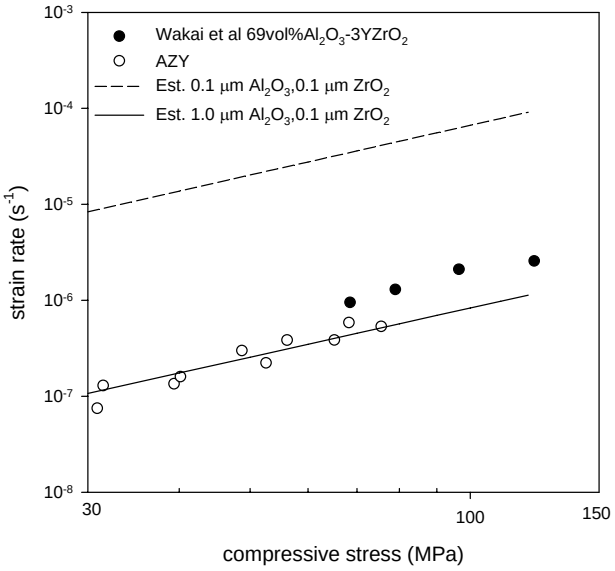

Figure 6. Comparison of creep results for AZY, results of Wakai et al. for 69 vol.% Al_2O_3 and with isostrain estimates from Al_2O_3 [10] for Al_2O_3 with Y_2O_3 and ZrO_2[11].

Creep rates measured from the forging experiments are compared in Fig. 6 to results of Wakai et al. [11] at 1250ºC for 69 vol.% (compared to 67 vol.% in our study). Their Al_2O_3 and ZrO_2 grain sizes were 0.99 μm and 0.59 μm, respectively. The solid and dashed lines assume a mixture of 67 vol.% Al_2O_3 and 34 vol.% ZrO_2 assuming isostrain composite creep. [12] Data is then taken from the literature for Al_2O_3[10] and for ZrO_2[11] and combined in the isostrain equation. The isostrain equation predicts that Al_2O_3 will dominate the creep behavior. The two cases considered here are 0.1 μm and 1.0μm grain size Al_2O_3. Based on this magnitude of creep comparison, it is concluded that the effective grain size of the Al_2O_3 phase controlling the creep behavior is on the order of 1.0 μm.

Thus far consideration has not been given to the early stages of densification. To consider the entire densification curve two methods were used for predicting $\dot{\rho}$ vs. ρ, where ρ is the relative density. The first is an analytical equation from Helle et al. [13] In the early stages (<90% dense)

$$\dot{\rho} = 3.1\rho^{\frac{2}{3}}\rho_0^{\frac{1}{3}}B\left(\frac{\sigma_a}{3\rho^2}\right)^n\left(\frac{1-\rho_0}{\rho-\rho_0}\right)^{n-\frac{1}{2}} \qquad (2)$$

B is the constant in the Norton equation $\dot{\varepsilon} = B\sigma^n$ and σ_a is the applied stress. At ρ>90%

$$\dot{\rho} = \frac{3}{2}B\left(\frac{3\sigma_a}{2n}\right)^n \frac{\rho(1-\rho)}{\left[1-(1-\rho)^{\frac{1}{n}}\right]^n} \qquad (3)$$

Figure 1. Finite element stress distribution of the upper right quadrant of a diametrical slice at two different stages of densification by creep.

The second method of predicting $\dot{\rho}$ vs. ρ is by a finite element technique developed with partial support from this program. In this method the distribution of elastic stresses within a 3-D spherical particle under diametrical z axis loading with lateral confinement is determined after a displacement, *dz*. Then each element is allowed to creep for a time period, *dt* and then the stresses are recalculated. The sequence is repeated in order to obtain a stress-density curve. A series of stress-density curves are generated at different displacement rates. The density at the same stress was picked from every curve and then the densification rate vs. density

was plotted for a pressure of interest. This analysis, therefore, assumed that the strain rate is independent of the load-strain rate history.

The resulting curves comparing experimental results of hot pressing AZY and sintered ZrO_2 spray dried spheres (described in paper II) in a silicon carbide die at 1350ºC are shown in Fig. 7. Excellent agreement is observed between experimental results and both methods of predicting the densification rate.

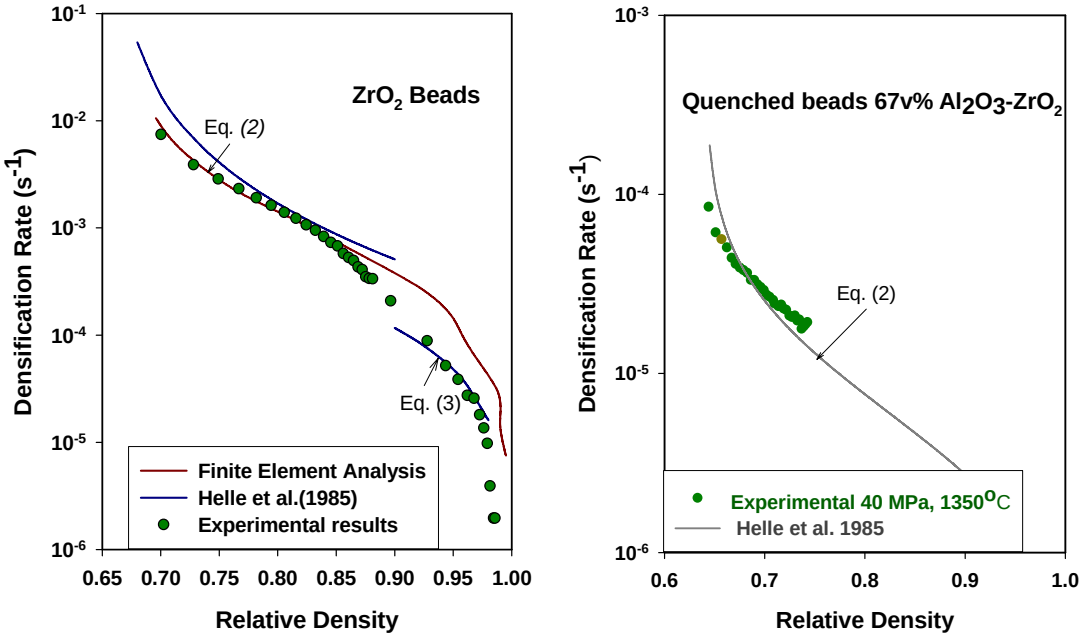

Figure 7. A comparison between experimental with Eqs (2) and (3) and with the FEM calculations at 1350ºC and 40 MPa for (a) ZrO_2 and (b) Al_2O_3-(1Y)ZrO_2 .

Based on the success of these equations to predict densification kinetics under hot isostatic pressure, the equations will be used to predict at what pressure powder might be pressed at 1150ºC, where a nanostructure is stable, in order to achieve full density. To do this a less simplified version of Eq. (2) is used which accounts for the temperature dependence. [14]

$$\dot{\rho} = c_1\left(\rho^2\rho_0\right)^{1/3}\left(\rho-\rho_0\right)^{1/2}\frac{\exp\left(-c_2/RT\right)}{kT\left[1+\left(T-300\right)/T_m\left(c_3\right)\right]^{c4-1}}\left(\frac{4\pi\rho\sigma_a}{3\left(\rho-\rho_0\right)\left[160\left(\rho-\rho_0\right)+16\right]}\right)^{c4} \qquad (4)$$

Tm is the melting temperature 1850ºC [15], c_1-c_4 are constants. From Fig. 6 at low temperatures the apparent activation energy, c_2=140 kJ/mol, and the shear modulus temperature dependence of Al_2O_3, c_3=0.35 [16]. The remaining two materials constants were then estimated by numerically searching for values that minimizes the sum of least squares between the experimental densification rates and those calculated by Eq. (4), utilizing the *fmins* function of MATLAB. The initial density was assumed to be ρ_0=0.64 and the influence of rearrangement was neglected. Results are shown in Fig. 8

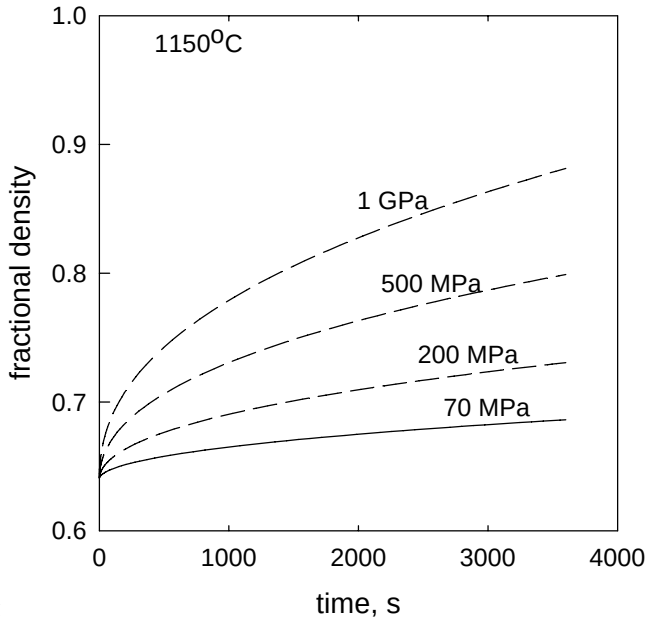

Figure 8. Predicted densification curve from Eq. (4) and constants determined from experimental densification curves at lower pressures and at several temperatures.

.

Forming Methods-Prospective:

Table II below lists the final densities achieved by the two step process of hot pressing then forging. Hot pressing alone in an alumina die at 1250ºC was not successful in achieving >80% of theoretical density. As described in the microstructural section, although some aspects of the microstructure were in the nanocrystalline regime (<100nm), the Al_2O_3 grains were much coarser. As described in the kinetics section, the coarser features controlled the densification behavior. In order to maintain a nano-nano structure (for optical transparency) forging or hot pressing at lower temperatures is required. Fig. 8 indicates that hot pressing in a die would require >1 GPa pressure to achieve densities >90% theoretical at 1150ºC for AZY. Attempts have been made to densify other compositions at low temperatures at pressures ~100 MPa but they either did not retain the nanomicrostructure or did not achieve high densities. McEnerney et al. [17] have succeeded in achieving 98% density of 80 vol.%Al_2O_3-20 vol.%$MgAl_2O_4$ by HIPping at 1260ºC for 6 hours and 207 MPa. We have tested some of their specimens and found the creep rates to be even lower than the AZY composition. Their microstructures, based on SEM images, appears to be in the scale of a few hundred nanometers, though insufficient studies have been completed to completely describe the microstructure. Based on this information it would appear that any of our compositions could likewise be made fully dense at 1260ºC by HIPping, however, these experiments have not been performed. One suggestion as to why such high densities are achieved by HIPping is that at higher stresses than were applied in our studies, the creep mechanism changes to power law and enhance densification kinetics.

Table II. Maximum fractional density achieved for each composition with corresponding compressive linear strain, initial stress and final stress

	1250ºC				1350ºC			
Material	Fractional Density	Linear Strain	Initial Stress	Final Stress	Fractional Density	Linear Strain	Initial Stress	Final Stress
AZ[1]	-	-	-	-	0.91	0.36	126	94
AZY	0.79	0.12	126	122	0.86	0.33	126	101
AZYG	0.85	0.57	133	97	0.89	0.94	125	48
SZY	0.97	0.86	190	106	0.98	1.40	203	70
SZYG	1.0	1.01	189	84	1.0	1.51	125	31
ASZY	0.88	0.70	190	147	0.93	1.05	190	69

A second alternative to achieving high densities is to apply large shear strains during hot forming. It is probably because of the high shear strains during forging vs. hot pressing that forging was much more successful in achieving high densities. It is believed that the presence of shear is more effective in filling porosity than isostatic pressure. In this program we have investigated hot extrusion in silicon carbide dies with the object of achieving full density through high shear strains. Also this process might be an economical one for forming sodium vapor lamp envelops, for example. Extrusion in silicon carbide dies with 80%, 90% and 95% reduction were attempted at 1250ºC. These extrusions were unsuccessful. High pressures cracked the die in one case and in others insignificant extrusion was observed. Also the compositions SZY, ASZY and SZYG reacted with silicon carbide and were difficult to remove from the die.

A more promising technology, which was studies towards the end of this program, was to hot press the specimen in the amorphous state below the crystallization temperature. This necessitates fully amorphous powder. As-quenched spherical fully amorphous powders were synthesized by adding La_2O_3. The eutectic La_2O_3-Al_2O_3-ZrO_2. (see reference 18) was fabricated. DTA revealed a strong exothermic peak beginning at 920ºC. Experiments in our laboratory showed that deformation rates increased rapidly to 920ºC and then fell off. Creep rates of the amorphous La_2O_3-Al_2O_3-ZrO_2 just below 920ºC were comparable to creep rates of the AZY composition at 1350ºC. A paper on this subject is in preparation. It is clear that formation of nano-crystallites in the amorphous matrix greatly retard densification rates. This method then is very promising since it holds the possibility of hot pressing or forging in metallic dies at moderate temperatures. The challenge is to raise the gap between the crystallization temperature and the glass transition temperature since this is the key to achieve sufficiently low viscosities.[18]

Summary and Conclusions

1. The microstructural evolution of as-quenched spherical powder particles of eutectic Al_2O_3-($1Y_2O_3$)ZrO_2 and the dense forged specimens were studied. Important observations were:
    a. As-quenched particles were partially amorphous-partially nanocrystalline. Crystallization occurred at 959ºC (exothermic peak) and above.
    b. Coarsening nanocrystalline microstructure was enhanced by deformation and occurred at 1200ºC and above. The final microstructure contained ~100 nm ZrO_2 particles in a matrix of Al_2O_3 with grain size on the order of 1 μm. Features designated as cells of 1-2 μm diameter were decorated with ZrO_2. These were believed to be higher energy Al_2O_3 grain boundaries to which ZrO_2 has migrated.
2. Densification occurred by creep under hot pressing and hot forging conditions.
    a. Creep rates during densification corrected for porosity were determined for six different compositions and found to follow an approximate n=1.5 stress dependence.
    b. A rapid decrease in the creep rate measured on powders in a die was observed between 1200ºC and 1300ºC for several compositions. This was believed to result from elimination of the final amorphous regions.
    c. Strain rates for the Al_2O_3-ZrO_2 eutectic composition agreed with literature creep results provided the effective grain size was ~1 μm in approximate agreement with microstructural observations.
    d. Densification kinetics followed Helle et al.[13] equations and also rates predicted by finite element analysis.
3. The densification rates at temperatures where the microstructure was entirely nanocrystalline, were not sufficient to achieve full density within a reasonable period of time.

References

1. W.R.Cannon, A.Petersson, C.Auechalitanukul, H.Keshavan, and A.Cuitino, "Hot-Pressing and Hot-Forging of Polycrystalline Powder Particles with Unique Microstructures," Submitted to CIMTEC 11th Internation Ceramic Congress, (2006).

2. H.Keshavan, A.Petersson, E.Pekarskaya, and W.R.Cannon, "Hot Forging of Spherical Beads with Nanocrystalline Microstructures: I Microstructure Development," unpublished (2006).

3. A.Petersson, H.Keshavan, and W.R.Cannon, "Forging of Spherical Beads with Nanocrystalline Microstructures: Kinetics of Densification," unpublished (2006).

4. Freim, J and McKittrick, J, "Modeling and Fabrication of Fine-Grain Alumina-Zirconia Composites Produced from Nanocrystalline Precursors," Journal of the American Ceramic Society, 81, 7, 1773-1780 (1998).

5. Bhaduri, S., Bhaduri, S. B., and Zhou, E, "Auto Ignition Synthesis and Consolidation of Al_2O_3-ZrO_2 nano/nano Composite Powders," Journal of Materials Research, 13, 1, 156-165 (1998).

6. Claussen, Nils, Lindemann, G, and Petzow, G, "Rapid Solidification in the Al_2O_3 - ZrO_2 System," Ceramics International, 9, 3, 83-86 (1983).

7. Bhaduri, S. and Bhaduri, S. B., "Microstructural and Mechanicl Properties of Nanocrystalline Spinel and Related Composites," Ceramics International, 28, 153-158 (2002).

8. Chen, I. W. and Xue, L. A., "Development of Superplastic Structural Ceramics," Journal of the American Ceramic Society, 73, 9, 2585-2609 (1990).

9. Langdon, Terence G., "Dependence of Creep Rate on Porosity," Journal of the American Ceramic Society, 55, 12, 630-634 (1972).

10. French, J. D., Zhao, Yongnian, Harmer, Marten P., Chan, Helen M., and Miller, G. A., "Creep of Duplex Microstructures," Journal of the American Ceramic Society, 77, 11, 2857-2865 (1994).

11. F.Wakai, Y.Kodama, S.Sakaguchi, N.Murayama, H.Kato, and T.Nagano, "Superplastic Deformation of Al_2O_3/ZrO_2 Duplex Composites," Proceedings of the MRS International Meeting on Advanced Materials, 7, 259-266 (1989).

12. Clarisse, L, Baddi, R, Bataille, A, Crampon, J, Duclos, R, and Vicens, J, "Superplastic Deformation Mechanisms during Creep of Alumina-Zirconia Composites," Acta Materialia, 45, 9, 3843-3853 (1997).

13. Helle, A. S., Easterling, K. E., and Ashby, M. F., "Hot-Isostatic Pressing Diagrams: New Developments," Acta Metallurgica, 33, 12, 2163-2174 (1985).

14. Arzt, E., Ashby, M. F., and Easterling, K. E., "Practical Applications of Hot-Isostatic Pressing Diagrams: Four Case Studies," Metallurgical Transactions A, 14A, 211-221-(1983).

15. Berezhnoi, A. S. and Kordyuk, K. E., "Melting Deagram of the System MgO-Al_2O_3-ZrO_2," dopovidii Akad.Nauk., 4, 506-508 (1964).

16. H. J. Frost and M. F. Ashby, "Deformation-Mechanism-Maps - the Plasticity and Creep of Meals and Ceramics," Deformation-Mechanism-Maps - the Plasticity and Creep of Meals and Ceramics, Pergamon Press, Oxford, (1982).

17. McEnerney, B. W., Quinn, G. D., Greenhut, Victor A., Sadangi, K, Shukla, V, Kear, B. H., and Niesz, Dale E., "Processing and Hardness of a Al_2O_3-$MgAl_2O_4$ Nanocomposite," Ceramic Science and Engineering Proceedings, 25, 4, 647-653 (2004).

18. Rosenflanz, A, Frey, M, Endres, B, Anderson, T, Richards, E, and Schardt, C, "Bulk Glasses and Ultrahard Nanoceramics Based on Alumina and Rare-earth Oxides," Nature, 430, 12 August, 761-764 (2004).

Publications and Presentations:

Publications

1. Chiraporn Auechalitanukul, Michael J. Roddy, and W. Roger Cannon (2004), "Plastic Densification and Grain Growth of Nanocrystalline Zirconia Powders, Ceramic Transactions Vol. 159, pp.137-144. (partially supported by the DOE grant).
2. S. Balasubramanian, H.Keshavan, and W. R. Cannon "Sinter-Forging of Rapidly Quenched Eutectic Al_2O_3-ZrO_2(Y_2O_3) -Glass Powders," J. Euro. Ceram. Soc. 26 1359-1364 (2005).
3. Sreeram Balasubramanian, Hrishikesh Keshavan, Chiraporn Auechalitanukul and W. Roger Cannon, Fabrication of Nanocrystalline Ceramics by Hot Pressing of Superplastically Deforming Powders," Sintering 03 Proceedings. Web Published.
4. Chiraporn Auechalitanukul and W. Roger Cannon "Densification of Single-grain vs Multi-grain Zirconia Powders," Proceedings of the 107th Annual Meeting & Exposition of The American Ceramic Society (2005). (partially supported by the DOE Grant)
5. A. Petersson, H. Keshavan and W. R. Cannon, "Microstructural Evolution and Creep Properties of Plasma Sprayed Nanocomposite Zirconia-Alumina Materials," Proceedings of the 107th American Ceramic Society Meeting CD publication.
6. W. R. Cannon**,** A. Petersson, C. Auechalitanukul**,** H. Keshavan**,** A. Cuitino, "Hot-pressing and Hot-forging of Polycrystalline Powder Particles with Unique Microstructures," Proceedings of CIMTEC 2006, 11th International Ceramics Congress (2006). Appendix.
7. H Keshavan, A Petersson, and W. Roger Cannon, "Hot Forging of Water Quenched Beads: Microstructure Development," Appendix
8. A Petersson, H Keshavan, and W. Roger Cannon, Hot Forging of Water Quenched Beads: Kinetics of Forging, in preparation.
9. Chiraporn Auechalitanukul, W. Roger Cannon and Alberto Cuitino, "FEM modeling for Hot Pressing of Spherical Powders by Creep," in preparation (partially supported by the DOE Grant)

Presentations

1. C Auechalitanukul , W. Roger Cannon, and A Cuitino "Effect of Particle Size and Particle Microstructure on Hot Pressing Zirconia Powders," Presented at the Materials Science and Technology 2005, Pittsburgh, PA, Sept. 2005
2. A. Petersson, H. Keshavan and W. R. Cannon, "Title," Presented at the Annual meeting of the Materials Science and Technology Conference, Pittsburgh, PA, Sept. 2005.
3. H, Keshavan, A. Petersson, and W. R. Cannon, "Title", Presented at the Annual meeting of the Materials Science and Technology Conference, Pittsburgh, PA, Sept. 2005. H. Keshavan, E Pekarshaya, A Petersson, and W. R. Cannon, "Densification of Eutectic Alumina/Zirconia with and without Glass," Presented at 29th International Conference & Esposition on Advanced Ceramics & Composites, Cocoa Beach, January 2005.
4. W. Roger Cannon, B. H. Kear, H Keshavan, E. Pekarskaya and S. Balasubramanian, "Hot forging of micron sized nano-structured Al_2O_3-ZrO_2 Powder," Presented at the 7th International Conference on nanostructured Materials, Wiesbaden, Germany, June 2004.
5. H. Keshavan, S Balasubramanian, and W. Roger Cannon, "Densification and Grain Growth in Al_2O_3-ZrO_2 Coarse Nanocrystalline Powder," Presented at the Annual Meeting of the American Ceramic Society, Indianapolis, IN, April 2004.
6. C Auechalitanukul and W. Roger Cannon, "Plastic Densification and Grain Growth of Nanocrystalline Zirconia Powder," Presented at the Annual Meeting of the American Ceramic Society, Indianapolis, IN, April 2004.
7. W Roger Cannon, "Microstructural Effects on Creep," International Workshop on Emerging Trends and Recent Developments in Cermics and Ceramic Matrix Composites, Coorg, Karnataka, India **invited presentation,** April 2004**.**
8. S Balasubramanian, C Auechallitanukul, H Keshavan and W.R Cannon, "Fabrication of Nanocrystalline Ceramics by Hot Pressing of Superplastically Deforming Powders," Presented at Sintering 03, Penn State University, September 2003.
9. "Sinter-Forging of Rapidly Quenched Eutectic Al_2O_3-$ZrO_2(Y_2O_3)$ -Glass Powders," Sreeram Balasubramanian, Hrishi Keshavan, and W. Roger Cannon, **invited presentation** at Ceramic Eutectic Workshop, May 2003, Paris, France.
10. Chiraporn Auechalitanukul, Sreeram Balasubramanian, and W. Roger Cannon, "Hot Pressing of Spherical Coarse Particle-Size Nanocrystalline Zirconia Powders ," Presented at the Annual Meeting of the American Ceramic Society, Nashville, TN, April 2003.
11. W R Cannon, "Synthesis and densification of Bulk Nanocrystalline Ceramics," **Invited presentation**, International Conference on Ceramic Processing, 8th ICCCP, Hamburg, Germany, September 2002.
12. W. R. Cannon, B. H. Kear, V. Shukla, X Zhou, "Metastable Zirconia-Yttria-Alumina Ceramics by Plasma Spraying," Presented at the Annual Meeting of the American Ceramic Society, St. Louis, MO, April 2002.
13. W. R. Cannon**,** A. Petersson, C. Auechalitanukul**,** H. Keshavan**,** A. Cuitino, "Hot-pressing and Hot-forging of Polycrystalline Powder Particles with Unique Microstructures," Proceedings of CIMTEC 2006, 11th International Ceramics Congress (2006).

Hot Forging of Spherical Beads with Nanocrystalline Microstructures: Microstructure Development

H. Keshevan, A. Petersson, E. Pekarskaya and W. R. Cannon
Materials Science and Engineering, Rutgers University

Abstract

As an alternate method of hot pressing or hot forging ceramics with a fine- or nano – scale microstructure, spherical beads 2-25 μm diameter (average 16 μm) obtained by a plasma melting spray dried powder and quenching into water were hot pressed and hot forged. Six different eutectic compositions in the Al_2O_3-$MgAl_2O_4$-Y_2O_3-ZrO_2-borosilicate glass system were studied. As-quenched beads contained both amorphous material and 20-40 nm crystallites (Al_2O_3-Y_2O_3-ZrO_2). The microstructure development of the Al_2O_3-(1%Y)ZrO_2 was followed during hot pressing and hot forging to full density. When fully dense after forging at 1350ºC the microstructure contained <100 nm ZrO_2 particles embedded an Al_2O_3 matrix of intertwined grains ~1 μm diameter . An additional feature cells about 2 μm diameter with ZrO_2 decorating the boundaries were observed.

Introduction

Typically nanocrystalline ceramics are sintered, hot pressed or hot forged from nanoparticulate powder. An alterative, which has recently been considered, is to hot press or hot forge micron sized spherical beads having nanoscale microstructures and then attempt to maintain that structure during densification. [1] [2,3] The advantage of this process over the nanoparticulate route is that powders are much easier to handle, do not hydrate or adsorb appreciable gases from the atmosphere, avoid health hazards associated with ingesting nanoparticulate powders and are easily formed to green bodies with densities on the order of 60% or more. The disadvantage is that the driving force for pressureless sintering is lost.

Provided the grain size within the particle is much smaller than the particle diameter, densification is by a creep deformation mechanism[1] such as Nabarro-Herring, Coble or superplastic creep. Therefore, densification by creep is controlled by the scale of the grain size, which dictates the diffusion distance, rather than the distance across the interparticle neck. It follows that the densification rate should be approximately independent of the particle size. Experimentally, we have shown that there is only a slight dependence on particle size due to differences in particle packing. [4] Thus there appears to be little advantage in hot pressing or hot forging nanoparticulate powder vs. micron sized powder with nanocrystalline microstructures. However, there are still some questions to be resolved.

Since the interior of the micron sized beads are not porous, there is no resistance to grain growth from the pore drag mechanism as is the case with nanoparticulate powders during sintering. Normally, as the sintered density approaches 85%-90% dense grain growth rate increases rapidly. [5] When dense beads are used the rapid grain growth rate might prevail during the entire hot pressing or hot forging process and a coarser grain

structure would result. This may also not be so since there is considerable difference in microstructure where nucleation and growth dominate the morphology rather than random mixing of powders.

Most of the studies of pressure-assisted densification of multigrain powder where the particle size is much larger than the grain size were performed on rapidly solidified (RS) powder. For instance, in references 1-5, spherical 5-25 μm-sized beads were synthesized by passing spray-dried agglomerates through an inert plasma flame above the melting temperature and rapidly quenching them in water. The most widely studied material is the Al_2O_3-ZrO_2 eutectic composition. The two-phase microstructure is found to be very to grain growth resistant. [6,7] For instance, Freim and McKittrick [8] observed ZrO_2 particles in Al_2O_3-ZrO_2 eutectic made from RS powders growing to no more than ~50 nm after annealing at 1650°C. The resistance of ZrO_2 particle growth by Ostwald Ripening, stems from the low solubility and low diffusion rate of Zr^{+4} in Al_2O_3 and from the uniformity with which it is dispersed in Al_2O_3. The uniformity of dispersion on the nanoscale is universal for RS powder quenched at rates of 10^3 to 10^4 °$Ksec^{-1}$. Since the crystalline phases nucleate and grow from the amorphous phase, as one phase nucleates the region around that phase is depleted leading to nucleation of the other phase. The scale of the phase size is directly related to the quenching rate.

There are other differences between microstructures formed from the melt and microstructures developed from sintered powders. First, heterophase boundaries in directionally solidified eutectics of Al_2O_3-ZrO_2 are low energy, strongly bonded and very stable. [9] It is likely that even RS powders quenched from the melt have low energy heterophase boundaries. Second, the as-quenched RS powder may be partially amorphous and partially crystalline and it is during the heat treatment or hot pressing that the crystalline microstructure fully develops. Third, additives are homogeneously distributed during the melt cycle and may not segregate to the grain boundaries. Fourth, the free energy driving force and the kinetics of reactions between components in heating to the sintering temperature differ from the higher temperature reactions during cooling from the melt. All in all, unique microstructures develop in hot pressed RS powders in contrast to milled and sintered parts.

There are several studies describing synthesis of RS powders but none have thoroughly studied the forging process or the development of the microstructure. Freim and McKittrick [10] quenched eutectic Al_2O_3-ZrO_2 molten droplets between stainless steel rollers. The RS quenched flakes contained a lamellar eutectic structure typical of very rapid quenching, with a lamellar spacing of less than 30 nm. When heated above 1400°C the lamellae were converted to equiaxed phases. As-quenched flakes were ground into particles 350 nm in diameter and sintered to full density between 1500°C and 1600°C. This technique was successful in developing a nanoscale interpenetrating network of Al_2O_3-ZrO_2 phases but there was no detailed discussion of the microstructure and whether this microstructure was uniform throughout the specimen. In an earlier work Freim and McKittrick [8] noted that RS powders were difficult to pressureless sinter because interconnected phases and low solubility. Only with shock-compacted ground RS flakes were they able to achieve 93-95% dense specimens. Little information was also reported about their microstructure. Bhaduri and Bhaduri [11 12] synthesized Al_2O_3-10% ZrO_2 by an auto ignition technique which is also an RS process yielding powder with nanocrystalline microstructures. After hot isostatic pressing specimens at 1200°C for

1 h at 247 MPa specimens were 99% dense and maintained the nanocrystalline microstructure with grain sizes ~30 nm.

The present paper describes the microstructural development of RS powders quenched at about 10^4 $^oKsec^{-1}$ from a plasma and the microstructure developed during hot forging. A number of microstructural features are reported which have not been reported in other papers. The Al_2O_3-ZrO_2 eutectic was studied since Al_2O_3 and ZrO_2 form a two-phase microstructure with little solubility in one another. Morita *et al* [13] added $MgAl_2O_4$ as a soft phase to increase grain boundary sliding and diffusion. They concluded that $MgAl_2O_4$ would supply Al^{3+} cations to the ZrO_2 matrix that is known to enhance the superplasticity of Y-TZP in tension and so the $MgAl_2O_4$-ZrO_2 binary eutectic and the Al_2O_3 rich Al_2O_3-$MgAl_2O_4$-ZrO_2 ternary eutectic compositions were also studied. In a companion paper the kinectic of densification by creep will be studied. Gust et al. [14]have shown that the creep rate of 3Y-TZP at high temperatures can be enhanced by adding as little as 0.5 wt% borosilicate glass and so a borosilicate glass was added to the two binary compositions.

Experimental Procedure

The starting powders were Al_2O_3 (Alcoa AG16-SG, Bauxite, AR), ZrO_2 (Magnesium Electron Inc., Manchester, England), alumina rich spinel (AR-78, Almatis Corp., Leetsdale, PA), MgO (MG-602, Atlantic Equipment Engineers, Bergenfield, NJ), Y_2O_3 (Unocal Molycorp, Mountain Pass, CA) and borosilicate glass (5.8% Na_2O, 1.6% K_2O, 1.6% Al_2O_3, 16% B_2O_3, 75% SiO_2) (Frit-492, Fusion Ceramics Inc., Carrowton, OH). The slurry for spraying drying was prepared by mixing the appropriate amount of ceramic powder with approximately 1-2 mass % of dispersant (Duramax D-3005, Rohm and Hass, Philadelphia, PA), which is an ammonium salt of polyacrylic acid of average molecular weight of 2000-3000 g/mol. No binder was used throughout the study. Yttria and borosilicate glass were attrition milled in de-ionized water for 2 hours to reduce the starting particle size. Magnesia was attrition milled in ethanol for 2 hours since it gels in water. The mean particle size (as determined by Coulter LS 230) for yttria, borosilicate glass and magnesia were all approximately 2 μm. Stoichiometeric magnesium aluminate spinel, $MgAl_2O_4$, was prepared by mixing alumina rich spinel to magnesia.

The six compositions studied are given in Table I. Theoretical densities in Table I were calculated by the rule of mixtures, assuming the theoretical densities of Al_2O_3 as 3.98 g/cm^3, ZrO_2 as 6.1 g/cm^3, magnesium aluminate spinel as 3.6 g/cm^3 and borosilicate glass as 2.4 g/cm^3. The ceramic powders with appropriate composition were mixed with de-ionized water and dispersant to obtain a slurry with 40 vol% solids loading. The slurry was ball milled for 20 h with zirconia grinding media and was spray dried (Niro Atomizer, Denmark) to obtain spherical agglomerates with particle diameters between 20 μm and 120 μm. Smaller agglomerates were collected in the cyclone and discarded. Agglomerates smaller than 75 μm were separated out by sieving and then calcined at 1000^{o}C for 4 h to impart strength to them prior to feeding them in the plasma arc gun. The powders were arc plasma melted (Northwest Mettech Corp., BC, Canada) and quenched into water. A radial powder injection, single electrode torch was used with power levels of 40 kW and a standoff distance of 200 mm. The porous agglomerate

completely melts and is rapidly quenched in water, which results in spherical, metastable, partially amorphous powder that is slightly smaller than the spray-dried agglomerates. Transparency under an optical microscope at 20X magnification was an indication of whether the agglomerate completely melted. It was found nearly 100% of the particles less than 25 μm were transparent for all the compositions. Hence, only this fraction was used for further study.

Table I Chemical compositions in mass % (vol.%)

Composition	Alumina	Zirconia	Magnesium aluminate spinel	Glass	Theoretical densities (g/cm^3)
AZY	57.8(67.3)	42.2 (32.6)[a]	-	-	4.7
AZ	57.8(67.3)	42.2(32.6)	-	-	4.7
AZYG	57.8(62.5)	42.2(30.2) [a]	-	4.0(7.2)	4.6
SZY	-	36.9(25.9) [a]	63.1(73.9)	-	4.1
SZYG	-	36.9(24.2) [a]	63.1(69.1)	4.0(6.57)	4.2
AZSY	25.2(29.6)	49.9(38.4)	24.9(31.9)	-	4.9

[a] stabilized with 1 mol % yttria

The plasma-sprayed powder was consolidated in two steps. It was first hot-pressed at conditions so that the fractional density obtained was 0.70 to 0.76. Hot-pressing conditions varied depending on the composition and are summarized in Table II. The pellets after hot pressing were between 3.5 mm and 4.4 mm high with a diameter of 7.3 mm for AZ and AZY and 4.5 mm for the rest of the compositions. The AZ and AZY must be pressed in a larger SiC die while all the others were hot pressed in Al_2O_3 tube and rods made into a temporary die.

Table II. Hot pressing conditions

Composition	Amount of powder weighed (g)	Temperature (^oC)	Stress (MPa)
AZY	0.6	1250	76
AZ	0.6	1250	76
AZYG	0.2	1250	45
SZY	0.17	1200	42.5
SZYG	0.2	1250	52.5
AZSY	0.2	1250	62.5

The pellets were sinter-forged at temperatures between 1150^{o}C to 1350^{o}C at initial stresses between 30 MPa and 125 MPa. Sinter forging was performed in a universal

testing machine under constant load (Instron 1361, Canton, MA) in a box furnace (CM furnace, Bloomfield, NJ). The load was applied to SiC push rods and the samples were forged between two polished SiC platens to minimize friction. The heating rate was 10 ^{o}K/min and the load was applied at constant displacement rate of 0.1 mm/min for AZY, AZ and AZYG and 0.2 mm/min for SZY and SZYG and AZSY so that maximum load was reached within 3 to 4 minutes. The sample was then forged for 60 minutes and was allowed to cool naturally.

Differential thermal analysis (DTA) was used to determine temperatures of crystallization and phase transformations. 0.45 g powder was used in each experiment with a coarse alumina powder as the reference. The heating rate was 10 ^{o}K/min to a maximum temperature of 1400°C.

X-ray diffraction (XRD, Siemens Kristalloflex D500, Cu Kα radiation, 40 kV, 30 mA) was used to determine phases present. Scanning was performed in the interval $20° \leq 2\theta \leq 90°$ at a rate of 0.03°/s with a dwell time of 2 s. The Kα2 signal was removed manually from the obtained patterns. The background intensity was not removed due to the uncertainty in the extent of the signal from the amorphous phase.

Microstructures were examined using both field emission scanning electron microscopy (FESEM, Zeiss Leo DSM 982 Gemini, Leo Gmbh, Germany) and transmission electron microscopy (Akashi beam technology, Japan, 200 keV). FESEM samples were prepared by mounting them in an epoxy, grinding and polishing down to 50 nm using diamond suspension. Two types of TEM samples were prepared. Forged samples were prepared by cutting into 2 mm by 2 mm by 3 mm and thinning to less than 7 μm with a wedge angle of 0.5729°. Thin sections of beads were prepared by mixing them in G1 epoxy (Gatan Inc., Pleasanton, CA). They were cut into 2 mm by 2 mm by 3 mm pieces and thinned to around 8 μm. Both types of samples were ion milled (Gatan Duomill Model 600, Pleasanton, CA) with 1 mA gun current and 6 kV gun voltage until the sample was electron transparent using argon as the milling medium.

Results

The diameter of the as-quench beads were < 25 μm, average 16 μm and the smallest approximately 2 μm and optically transparent as shown in Fig. 1.

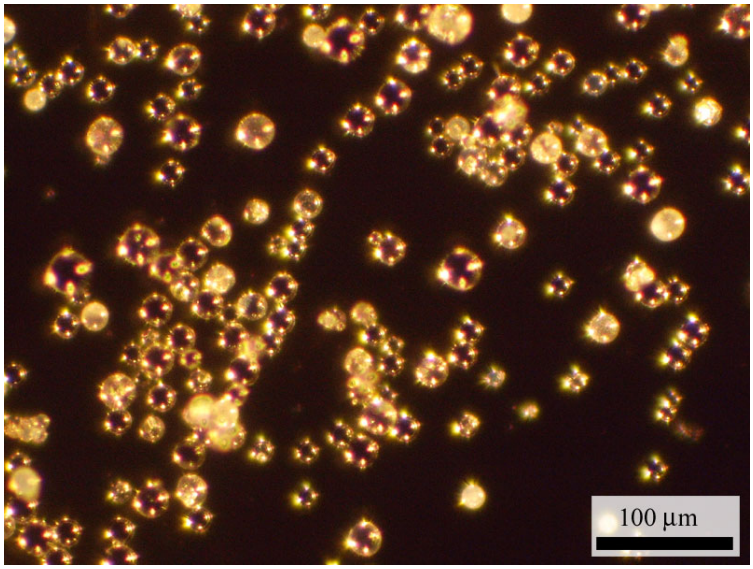

Fig. 1. Typical optical micrograph of spray-dried powder after passing through a plasma flame and rapidly quenching into water.

XRD pattern of AZY at three different conditions are shown in Fig. 2 to illustrate the phase evolution during annealing. A summary of phase development of all compositions is shown in Table III. As-quenched plasma sprayed powder shows broad reflections of *t*-ZrO_2 peaks in compositions containing Al_2O_3 and c-ZrO_2 peaks in compositions containing $MgAl_2O_4$. In the latter the c-ZrO_2 derives from absorption of sufficient MgO from the spinel phase to stabilize the c-ZrO_2. [15] XRD patterns indicate the presence of amorphous material in the as-quenched beads. Analysis of the amorphous hump indicated that the as-quenched beads were between 30-40% amorphous. After heat to 1200°C the amorphous fraction decreased to less than 10%. Peaks of γ-Al_2O_3 are also seen in AZ, AZY and AZYG as-quenched powder. (We were unable to definitely distinguish between γ-Al_2O_3, δ-Al_2O_3 and θ−Al_2O_3 and so will subsequently be referred to as γ-Al_2O_3). When annealed above 1250°C, the peaks were much narrower and *c*-ZrO_2 transformed to *t*-ZrO_2 in compositions containing $MgAl_2O_4$.

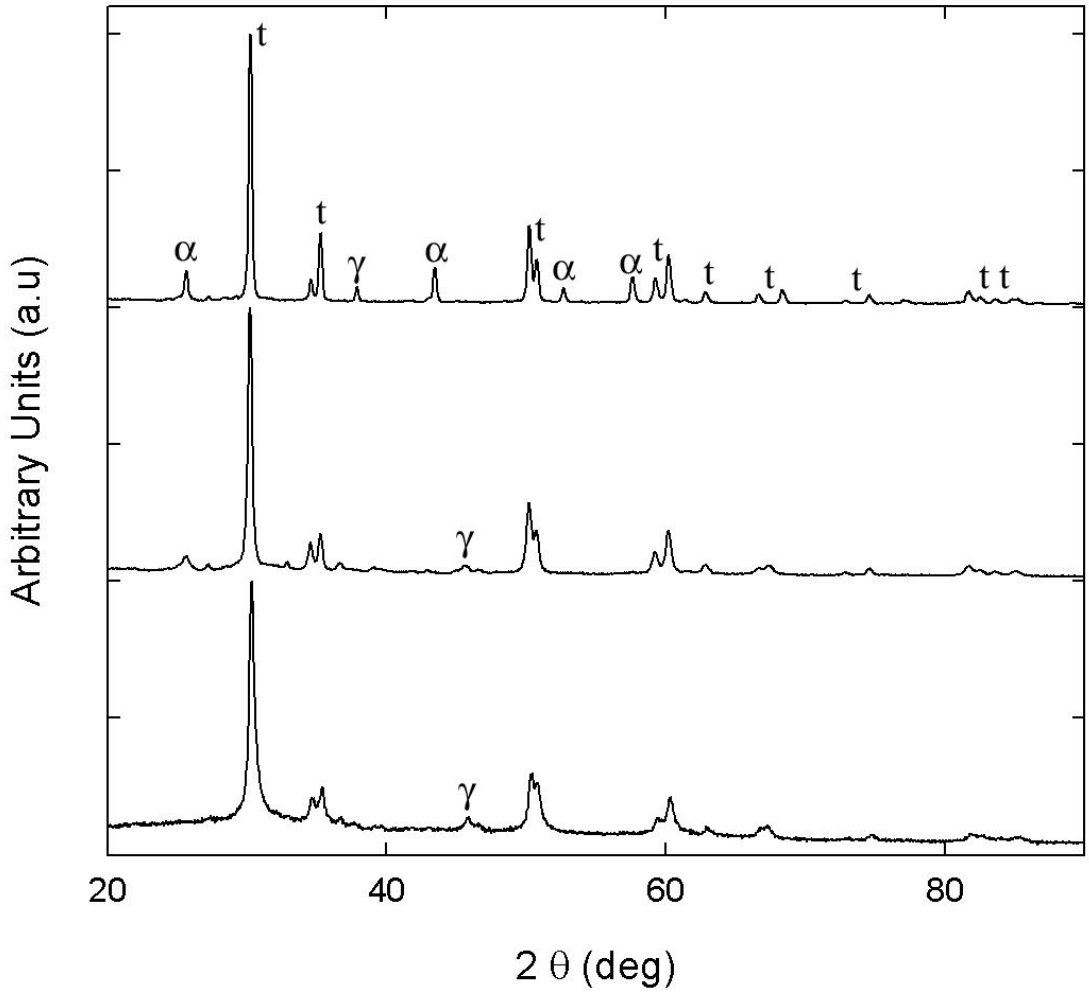

Fig. 2. XRD patterns of (a) as-quenched plasma-sprayed powder (b) annealed at 1250 ^{o}C for 30 minutes (c) annealed for 1350 ^{o}C for 1 h

Table III. Phase evolution for all the compositions illustrating phase transformation in hot pressing and sinter-forging

Composition	As received	1250 ^{o}C 30 minutes	1350 ^{o}C 60 minutes
AZ	t-ZrO_2, γ-Al_2O_3	t-ZrO_2, γ-Al_2O_3	t-ZrO_2, α-Al_2O_3
AZY	t-ZrO_2, γ-Al_2O_3	t-ZrO_2, γ-Al_2O_3	t-ZrO_2, α-Al_2O_3
AZYG	t-ZrO_2, γ-Al_2O_3	t-ZrO_2, γ-Al_2O_3	t-ZrO_2, α-Al_2O_3, $ZrSiO_4$
SZY	c-ZrO_2, $MgAl_2O_4$	t-ZrO_2, $MgAl_2O_4$	t-ZrO_2, $MgAl_2O_4$
SZYG	c-ZrO_2, $MgAl_2O_4$	t-ZrO_2, $MgAl_2O_4$, $ZrSiO_4$	t-ZrO_2 $MgAl_2O_4$, $ZrSiO_4$
AZSY	c-ZrO_2, $MgAl_2O_4$ γ-Al_2O_3	t-ZrO_2, $MgAl_2O_4$, δ-Al_2O_3, α-Al_2O_3	t-ZrO_2, $MgAl_2O_4$, α-Al_2O_3

Crystallization of the amorphous phase was studied by DTA. (Fig. 3) The results of the onset temperatures and peak temperatures for all the compositions are tabulated in Table IV. An intense exothermic peak corresponding to crystallization was seen in AZ, AZY and AZYG between ~930° and ~970° C. [16]A much broader peak was observed for crystallization of SZY and SZYG between 820 and 900° C. The exothermic peak between 830 and 861°C for ASZY was intermediate in width and height. DTA peaks for AZ and AZYG were similar to AZY and SZYG was similar to SZY. The small exothermic peak in AZY between 1306 and 1340°C arises from the γ–Al_2O_3 to α-Al_2O_3 phase transition. A second small peak is also present in SZYG between 954 and 960° C due to formation of $ZrSiO_4$. In the as-quenched Al_2O_3-ZrO_2, mass ratio by Rietveld analysis results in a 1.1:1 ratio in the as-quenched powder, but only (0.7-0.8):1 after heating to 1000°C indicating that relatively more ZrO_2 crystallized than Al_2O_3. XRD intensity ratios agree fairly well with this conclusion. However, Al_2O_3 is important for the crystallization event, as evident from the composite DTA (Fig. 3) showing a narrower crystallization range at higher temperature than for the spinel-ZrO_2 compositions. Based on eutectic there should be a 1.37:1, Al_2O_3:ZrO_2 ratio and so additional Al_2O_3 crystallizes out above 1000°C. DTA shows the onset of crystallization between 821 °C for SZY and 935 °C for AZYG, respectively. At this temperature it is possible that there might be a number of simultaneous nucleating events occurring in the powder in which one of the components nucleates and depletes the surrounding of that component which will aid in the nucleation of the other component.

Usually an endothermic peak corresponding to the glass transition temperature, T_g, is present in RS Al_2O_3-ZrO_2 just below the crystallization temperature, T_x. According to Rosenflanz et al [17] T_g occurs too close the T_x to be seen.

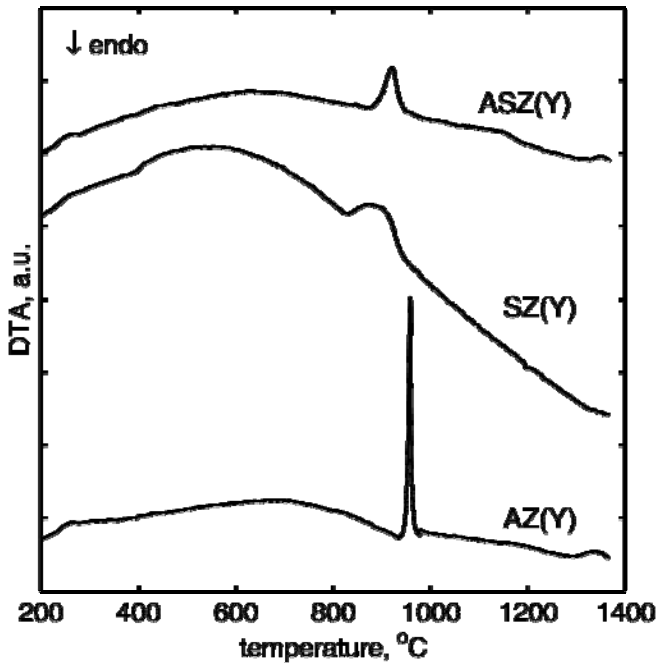

Fig. 3. DTA of ASZY, SZY and AZY.

Table IV. DTA peak positions for the various compositions.

Composition	Onset Temperature 1 (^{o}C)	Peak Temperature 1 (^{o}C)	Onset Temperature 2 (^{o}C)	Peak Temperature 2 (^{o}C)
AZ	931	965	1243	1282
AZY	932	959	1306	1340
AZYG	935	971	1283	1322
SZY	821	900	-	-
SZYG	830	861	954	960
ASZY	888	921	1329	1356*

Fig. 4 shows TEM micrograph of the as-quenched AZY plasma-sprayed powder. The crystallite sizes range from 50 to 80 nm. The inset shows a selected area diffraction (SAD) pattern of the starting powder. Both diffused and spotted rings are seen which suggests that the crystallites are dispersed in an amorphous phase. Fig. 5 shows a TEM micrograph of AZY powder that was heated to 1250 ^{o}C and cooled naturally. The crystallites are much smaller, ranging from 20 to 40 nm, and more faceted. It may be that the smaller crystallites, preferentially ZrO_2, crystallized near T_x whereas in the as-quenched beads crystallization was at a higher temperature. The absence of the larger crystallizes after annealing, however, leads us to suspect that a smaller particle was randomly chosen for the annealed bead, which lead to the difference in crystallite size.

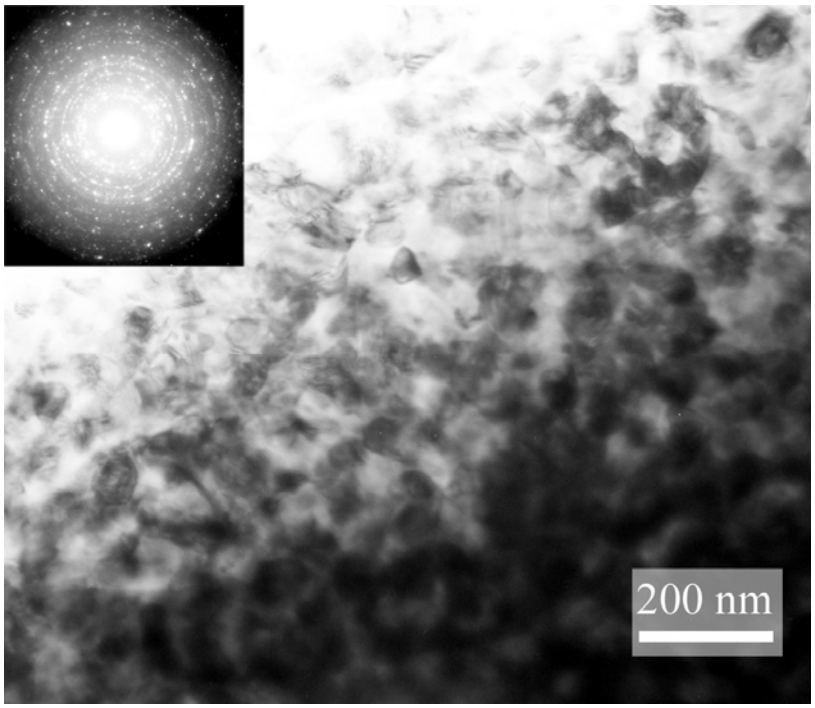

Fig. 4. Bright field TEM micrograph and SAD of the starting AZY powder in epoxy showing typical crystallite size 50-80 nm. Light phase is alumina and dark phase is zirconia.

* XRD shows α-Al_2O_3 forming between 1200°C and 1250°C during heating.

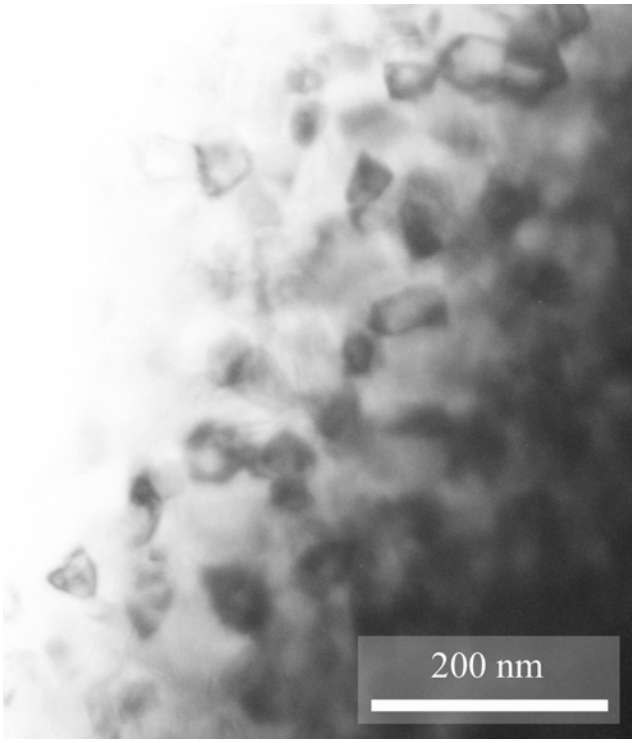

Fig. 5. Bright field TEM image of AZY heated to 1250 ^{o}C and cooled naturally. Typical crystallite size is 20–50 nm. Light phase is alumina and dark phase is zirconia.

SEM studies of as-quenched partially-amorphous plasma-sprayed powder did not reveal any surface microstructure. That is, no contrast between Al_2O_3, the dark phase, and ZrO_2, the light phase, was evident even at the highest magnifications. (The resolution for contrasting Al_2O_3 from ZrO_2 phase is limited to a few tens of nanometers because secondary electron scattering from phases below the surface.) However, when the powder was annealed at 1200 ^{o}C for 4 h, cell like domains were visible on the surface of powder. The boundaries of these cell-like domains were decorated by stringers of zirconia particles. (Fig. 6 a). Powder without glass (AZ, AZY, SZY and AZSY) formed equiaxed cell-like domains as shown in Fig. 6(a), whereas those with glass (AZYG and SZYG) formed nonequiaxed cells as shown in Fig. 6(b). Higher magnification of all compositions revealed a bi-continuous polyphase structure such as shown in Fig. 6(c) and (d). However, these features are only seen on the surface of the particles. We polished cross sections of the beads and have not observed the ZrO_2 decorated boundaries but only at a higher magnification have we observed the fine phase structure. It became clear from higher temperature annealing under stress studies that these microstructural features appeared first on the surface and grew into the interior and it appeared that they nucleated preferentially at points of high stress.

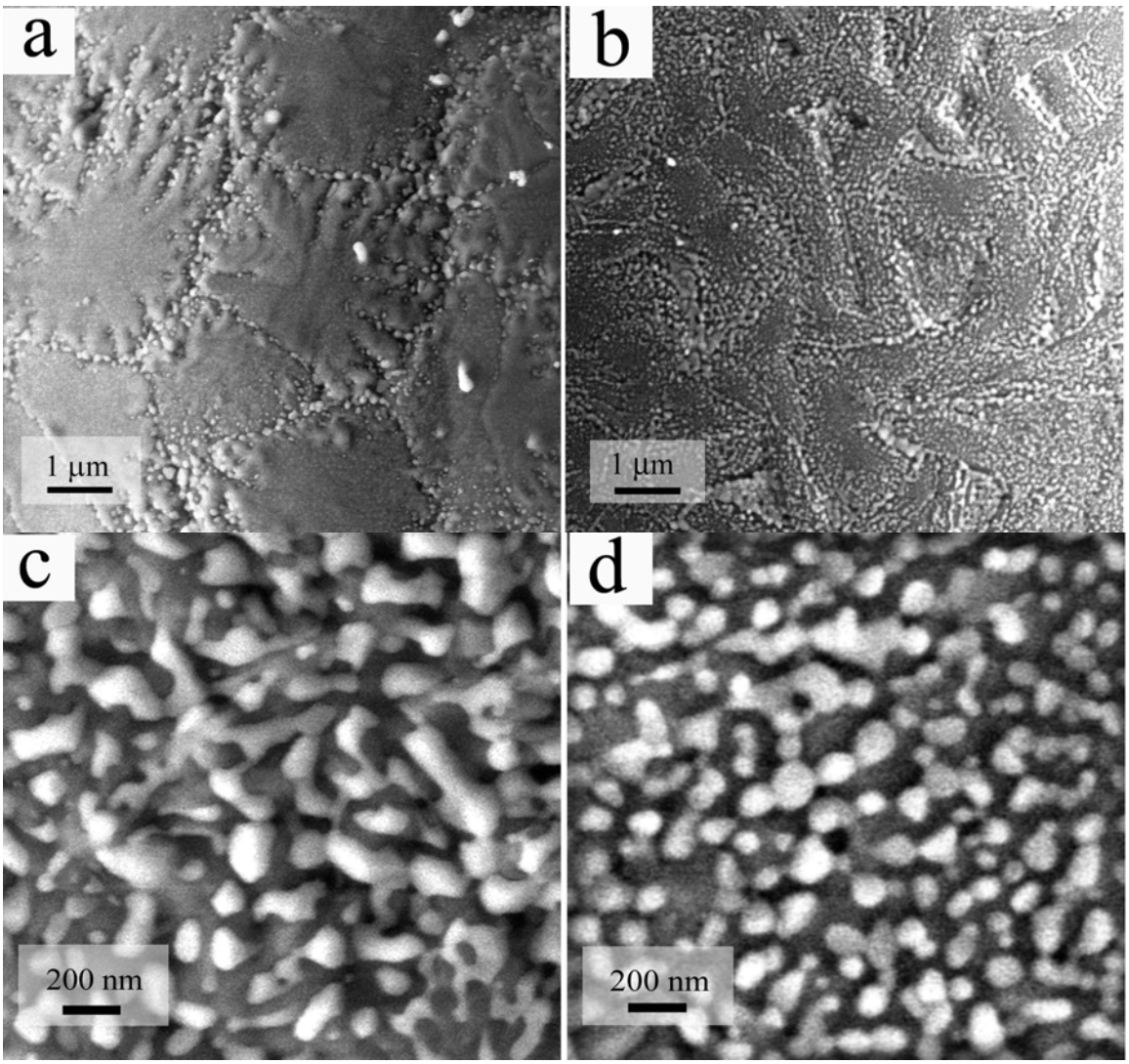

Fig. 6. Secondary electron FESEM micrographs showing starting powder annealed at 1200 °C for 4 h. Note the cell-like sub-domain in (a) and plate-like sub-domain in (b) with the addition of glass. (c) and (d) Higher magnification of (a) and (b) respectively. Light phase is zirconia and dark phase is alumina.

Most of the compositions could be forged to >90% dense at 1350°C in one hour at ~50 MPa. SZY consistently exceeded 99% density. The density of most other composition varied from fully dense in the center to porous around the outside. The spinel containing compositions and those with borosilicate glass added densified the fastest. A more complete discussion of kinetics will be presented in a future paper. [18]Low magnification microstructures of the five compositions after sinter-forging at 1350 °C for 1 h at ~50 MPa are shown in Fig. 7. AZ is not shown since it has a similar microstructure to AZY. Note how the spherical particles have changed shape to fill in the voids. It appears that some particles are softer than others perhaps because of varying composition between particles. In Fig. 7(b) an originally spherical particle from AZYG

that was deformed very little can be seen in the bottom left, whereas, the rest of the micrograph have particles that are plastically deformed beyond recognition. The densification rates of AZ and AZY are less than the other compositions at any temperature and stress and hence are at a much earlier stage of densification. In AZY and SZY, Fig. 7(a) and 7(c), all the domains are equiaxedally-shaped with sizes typically around 2 μm.

The compositions that contain glass have two types of domains in their microstructures. They have cell-like domains that are similar to AZY and SZY with typical cell sizes around 2 μm. In addition to this they have cells that are typically 2–3 μm long and around 0.5 μm wide as shown in Fig. 7(b) and Fig. 7(d). This seems to indicate that they are 2-D plates. The only features that are coarser than ~100 nm are the ZrO_2 phase delineating the cell boundaries. It is noted that these are much coarser in the microstructures containing glass and especially in SZYG (Fig. 6(d)) and next most in those containing spinel.

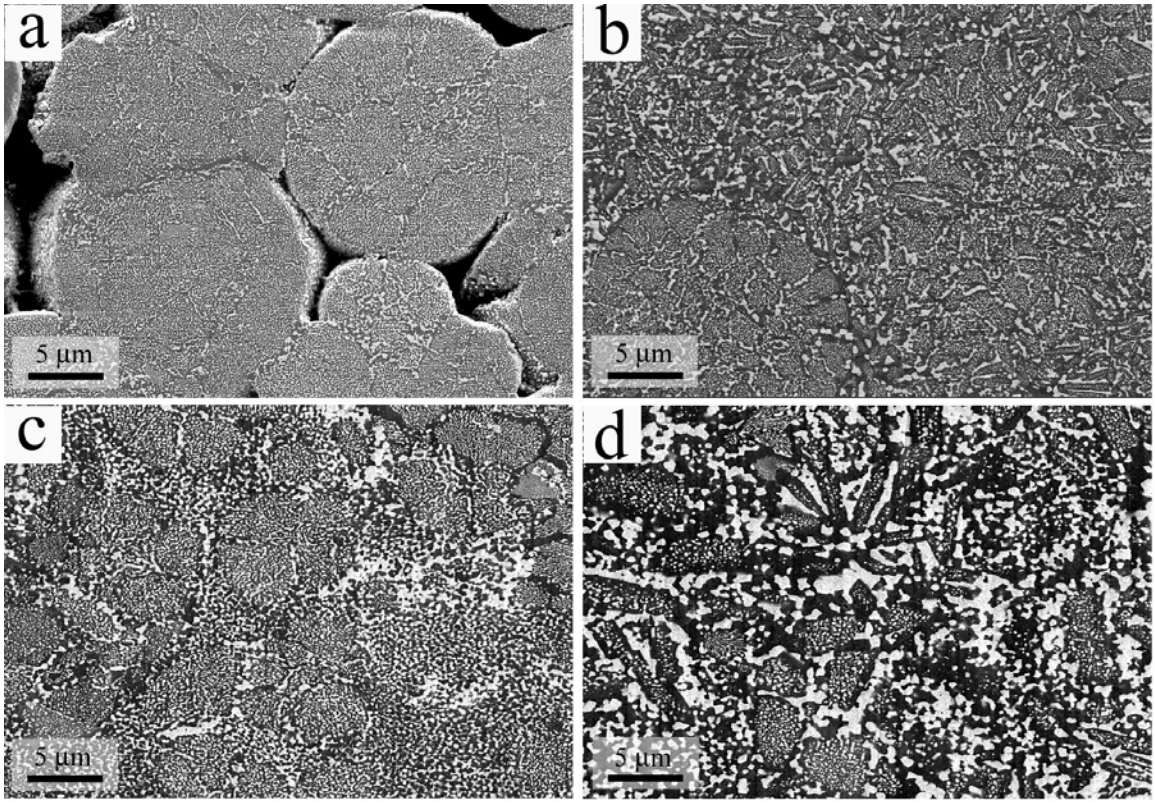

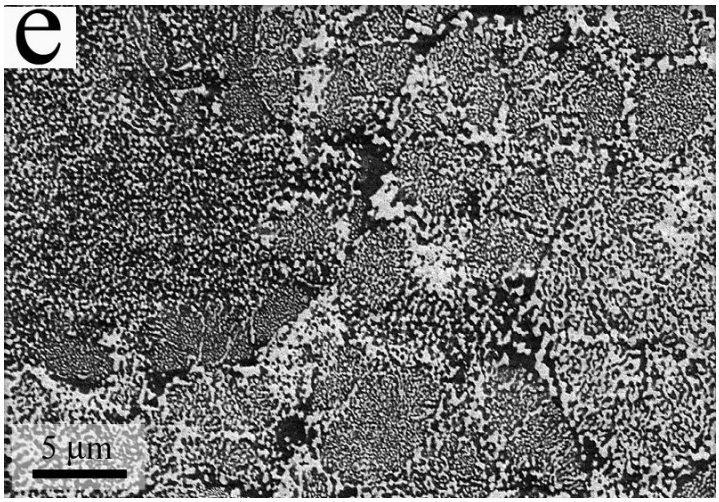

Fig. 7. Secondary electron FESEM micrographs of samples forged at 1350 °C for 1 h at ~50 MPa similar final effective stress. Light phase is zirconia, dark phase is alumina in AZY and AZYG and $MgAl_2O_4$ in SZY and SZYG. (a) AZY, (b) AZYG, (c) SZY, (d)SZYG and (e) ASZY.

Fig. 8 shows a TEM image the AZY specimen shown in Fig. 7(a) with four cell-like domains labeled A through D. The four domains are separated by stringers of ZrO_2 particles, some of which are intimately connected. Within these cell-like domains are nano-sized zirconia particles with multiple crystallographic orientations. From SAD, however, it is clear that Al_2O_3 has a single orientation in each cell leading to the conclusion that these are Al_2O_3 grains and the ZrO_2 stringers decorate the grain boundary. SAD patterns where the aperture is directly over a grain boundary indicate two Al_2O_3 orientations. The ZrO_2 phase within the grains have many different crystallographic orientations though because of the high volume fraction must be interconnected and contain multiple grains. Along the Al_2O_3 grain boundary the ZrO_2 is often polycrystalline.

Fig. 9(a) shows a TEM image of a part of an AZYG equiaxed grain of the type shown in Fig 7(b), however after forging at 1250°C rather than 1350°C. TEM imaging and SAD analysis also show a single orientation for the Al_2O_3 matrix and multiple orientations for nano-sized zirconia particles dispersed in the micron-sized alumina matrix grain. As mentioned before, compositions with glass have both equiaxed grains and nonequiaxed grains, which appear to be plate-like. Fig. 9(b) shows a part of a AZYG plate that has equiaxed nano-sized ZrO_2 particles down the center but with a zone near the grain boundary denuded of ZrO_2. Furthermore, in these samples the ZrO_2 decoration along the grain boundary is quite thick. Figure 9(b) shows that these grain boundary regions are polycrystalline ZrO_2.

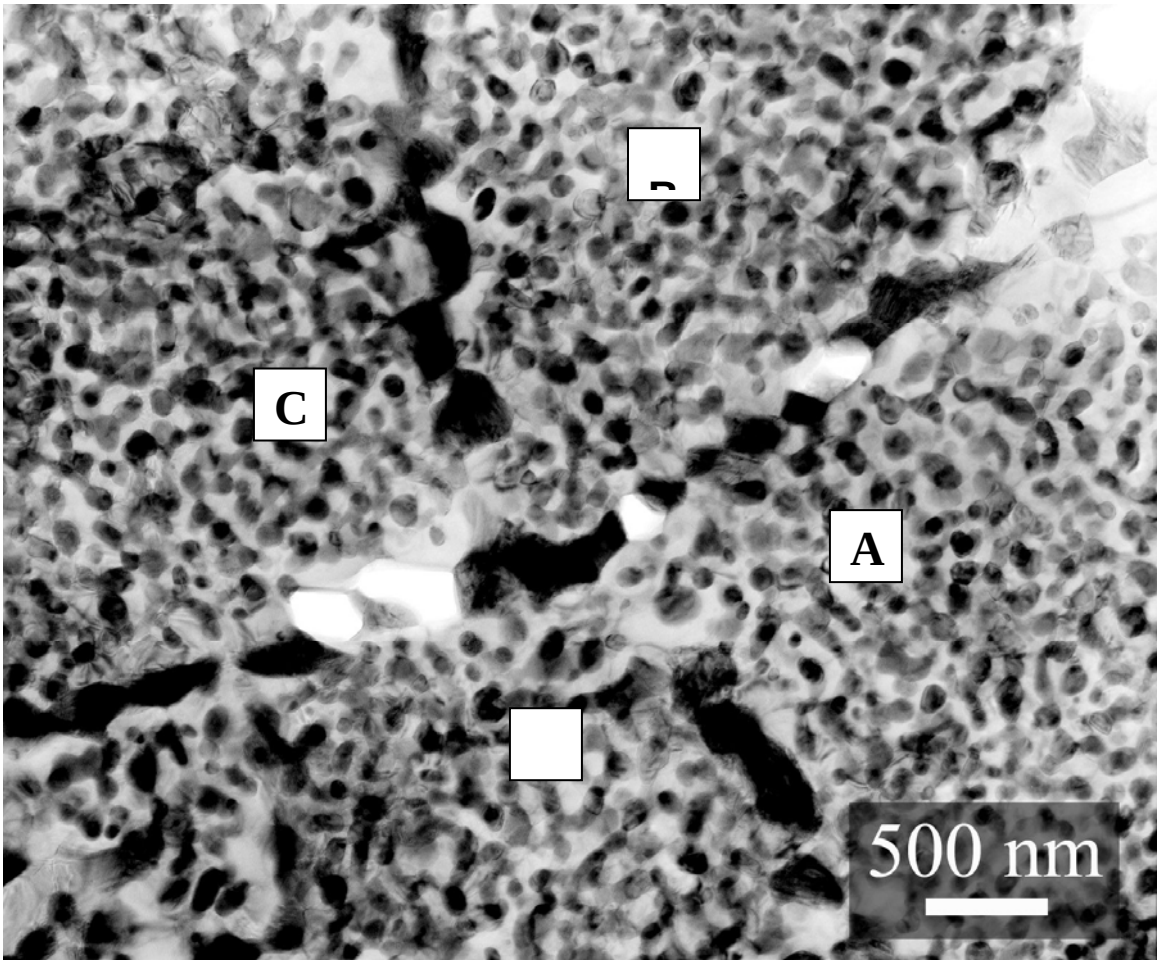

Fig. 8. TEM image of AZY showing four cells forged at 1350°C. SAD confirmed that nano-sized polycrystalline zirconia (dark phase) are dispersed in an alumina matrix (light phase) typically around 2-4 μm. Grain boundary can be distinguished by polycrystalline zirconia stringers.

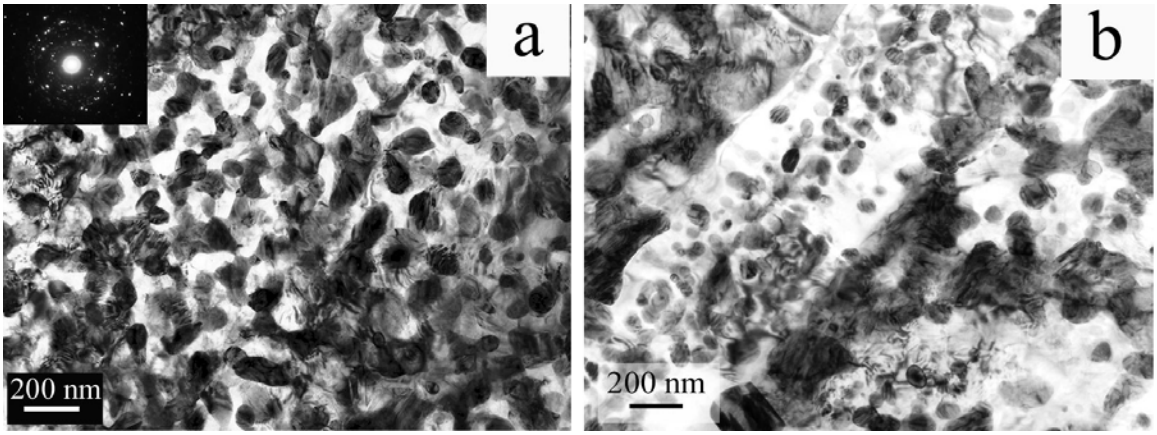

Fig. 9. TEM image of AZYG (a) cell that shows equiaxed polycrystalline and nano-sized zirconia (dark phase) embedded in sub-micron alumina grain (light phase) (b) plate having nano-sized polycrystalline zirconia in an alumina grain.

TEM studies have also been performed on the spinel containing compositions. Similar conclusions were reached, i.e. that polycrystalline ZrO_2 decorated the grain boundaries between spinel grains and that ZrO_2 particles within the grain had multiple orientations.

Discussion

The intent of this study was to hot press or hot forge specimens from beads containing nanocrystalline microstructures with the hope that the nanocrystalline microstructure might be maintained. All the materials reported here after being fully densified at 1350°C have a nanoscale distribution of phases over at least some portion of the microstructure. Never the less, there are features which are much coarser, especially the dimensions of the Al_2O_3 and spinel grains. Furthermore, it will be shown in a future paper [18]that the kinetics of densification are dependent on the scale of the grain size and not the ZrO_2 particle size or the phase spacing. It is thus of interest to follow the development of the grains. There are three important stages in the development of the scale of the microstructure. As the beads are water quenched crystallites begin to grow somewhere below the eutectic temperature, ~1860°C and during the approximately one second quench to T_g. In that time Al_2O_3 and ZrO_2 must segregate for nucleation and growth of crystallites of 20-30 nm. The SAD pattern shown in Fig. 4 clearly indicates the polycrystalline nature of the as-quenched particle. Never the less, some spots are rather bright and considering the number of grains within the selected area, there may be interconnected crystallites of the same orientation over a hundred nanometers. In contrast, the SAD for dense, forged microstructures in Figs. 8 and 9 have a single crystalline α-Al_2O_3 pattern over the same sized area. However, TEM of annealed powder particles below the temperature for the formation of α-Al_2O_3 indicate the crystallite size is 20-40 nm. Thus growth of the grains occurred primarily during the γ-Al_2O_3 to α-Al_2O_3 phase transformation. Observations of growth from nanometer γ-Al_2O_3 crystallites to micron-sized α-Al_2O_3 have been made by a number of investigators, for example, Chou and Nieh [19] In microstructures described in this paper, growth of the ~2 μm grains occurred by growing past 50 nm diameter ZrO_2 particles, some of which must be interconnected. There is a question, however, at what point does the growth of spinel grains occur since there is no transformation near 1200°C that leads to the growth of grains. It is our observation that the kinetics of grain growth are merely faster and growth is rapid above ~1200°C.

Stringers of ZrO_2 particles or a continuous polycrystalline ZrO_2 phase decorated the grain boundary. Sometimes there was a zone to either side of the grain boundary denuded of ZrO_2 while the grain boundary itself was a continuous polycrystalline ZrO_2. This was especially true in compositions containing glass. One possible mechanism is that during grain growth, grain boundaries sweep particles with them. However, the formation of α-Al_2O_3 in the AZY composition takes place before the decoration of the grain boundaries with ZrO_2. Furthermore, Chou and Nieh [19] showed that growth of α-Al_2O_3 was by rotation and coalescence of nonanocrystalline γ-Al_2O_3 grains rather than

sweeping of an α-Al_2O_3 phase boundary. This is probably true for the spinel containing compositions as well. TEM images of spinel containing compositions at 1250°C sometimes show the presence of larger grains without an excess of ZrO_2 along the grain boundary. It appears then that ZrO_2 on either side of the grain boundary migrate to the grain boundary. In cases where there was either no denuded zone or only a slight denuded zone, it is possible that ZrO_2 is supersaturated in the Al_2O_3 matrix after quenching and especially near grain boundaries [20], came out of solution between 1250 and 1350° C. The thermodynamic driving force for segregating to the grain boundaries is to minimize interface energy. Chen and Xue [21]examined a large number of dihedral angles in Al_2O_3-ZrO_2 composites. They concluded that the interface energy was in the order $\gamma_{Al_2O_3-Al_2O_3} > \gamma_{Al_2O_3-tZrO_2} > \gamma_{tZrO_2-tZrO_2}$. Thus a ZrO_2 particle on the boundary reduces the area of the Al_2O_3-Al_2O_3 boundary without changing the Al_2O_3-ZrO_2 interface area. An even greater driving force is available when a polycrystalline Al_2O_3-ZrO_2 interface is replaced by a ZrO_2-ZrO_2 grain boundary.

The role of the borosilicate glass is to enhance the kinetics of microstructure development, presumably by enhancing both grain boundary and bulk diffusion due to aliovalent ions. The borosilicate glass also had the side effect of altering the morphology of the phases. Glassy grain boundary phases often produce preferred growth planes. Although we have performed HRTEM on specimen AZYG we have been unable to see a glassy phase at the grain boundaries or triple points. Never the less, we believe glass exists at the grain boundary because of the morphology. However, after annealing at 1350 ^oC XRD patterns showed trace amount of $ZrSiO_4$ peaks and that the silica reacted with the ZrO_2 phase. The effect of glass should be different for compositions quenched from the melt from those where the glass is mixed with the powder and heated to the sintering temperature. First, in the latter case the glass starts at the surface of the particle and then later becomes part of the grain boundary. Second, it never sees a higher temperature. Finally, the free energy of $ZrO_2 + SiO_2 \rightarrow ZrSiO_4$ is much higher near the melting point than near the sintering temperature. The final two reasons may not have been important since $ZrSiO_4$ was not detected until after heating to 1250°C. Mullite peaks were only observed after forging to 1350°C.

By applying a higher stress it should be possible to densify the nanocrystalline microstructure to full density. This is a matter of creep rate kinetics and the microstructure controlling creep at the densification temperature. This will be discussed in a future paper. [18]

Conclusions

Microstructures resulting from hot pressing and hot forging quenched eutectic beads is quite different from the microstructures reported in the literature of either binary and ternary eutectic compositions when the component powders are merely mixed, pressed into shape and sintered or hot pressed. This must be due to more thorough mixing of the components, different starting powder and perhaps different thermal history if the quenching cycle is considered. When densified below 1200-1250°C the microstructures of the six compositions studied were all quite uniform and nanostructured

but not fully dense. Above this temperature some compositions could be forged to >99% density but as γ-Al_2O_3 converted to α-Al_2O_3 grains grew to 1-2 μm diameter while still maintaining the ~50 nm spacing of ZrO_2 phase within the interior of grains. Above 1250°C ZrO_2 particles or polycrystalline phase decorated the grain boundaries of the Al_2O_3. Behavior was only slightly different in the spinel-ZrO_2 binary even though there was no transformation similar to γ-Al_2O_3 to α-Al_2O_3 one. In this case there was apparently a higher rate of diffusion allowing grain growth to occur.

Acknowledgement

Financial support for this work came from Basic Energy Sciences Division of the Department of Energy Grant Number DE-FG02-O2ER46010. We wish to thank B. Kear and S. Balasubramanian for helpful discussions.

References

1. S. Balasubramanian, H. Keshavan, and W. R. Cannon, "Sinter-Forging of Rapidly Quenched Eutectic Al_2O_3-ZrO_2(Y_2O_3) -Glass Powders," J.Eur.Ceram.Soc., **26**, 1359-1364, (2005).

2. C Auechalitanukul, S Balasubramanian, and W. R. Cannon, "Hot Pressing of Nanocrystalline Y-ZrO_2 using Large Spherical Powders," unpublished work.

3. X. Zhou, D. M. Hulbert, J. D. Kuntz, K. Sadangi, V. Shukla, B. H. Kear, and A. K. Mukherjee, "Superplasticity of Zirconia-Alumina-Spinel Nanoceramic Composite by Spark Plasma Sintering of Plasma Sprayed Powders," Materials Science and Engineering A, **394**, 353-359, (2005).

4. C Auechalitanukul, A Cuitino, and W R Cannon,"Hot Pressing of Multigrain ZrO_2 Beads: Particle Size Dependence," unpublished work.

5. T. K. Gupta, "Possible Correlation Between Density and Grain Size During Sintering," J. Amer. Ceram. Soc., **55**, [5], 276-277, (1972).

6. J. D. French, M. P. Harmer, H. M. Chan, and G. A. Miller, "Coarsening-Resistance Dual-Phases Interpenetrating Microstructures," J. Amer. Ceram. Soc., **73**, [8], 2508-2510 (1990).

7. K. B. Alexander, P. F. Becher, S. B. Waters, and A. Bleier, "Grain Growth Kinetics in Alumina-Zirconia (CeZTA) Composites," J. Amer. Ceram. Soc., **77**, [4], 939-946 (1994).

8. J. Freim and J. McKittrick, "Development of Novel Microstructures in Zirconia-toughened Alumina using Rapid Solidification and Shock Compaction," J. of Mater. Res., **11**, [1], 110-117 (1996).

9. A. Sayir and S. C. Farmer, "The Effect of the Microstructure on Mechanical Properties of Directionally Solidified $Al_2O_3/ZrO_2(Y_2O_3)$ Eutectic," Acta Materialia, **48**, 4691-4697 (2000).

10. J. Freim and J. McKittrick, "Modeling and Fabrication of Fine-Grain Alumina-Zirconia Composites Produced from Nanocrystalline Precursors," J. Amer. Ceram. Soc., **81**, [7], 1773-1780 (1998).

11. S. Bhaduri and S. B. Bhaduri, "Enhanced Low Temperature Toughness of Al_2O_3-ZrO_2 nano/nano Composites," NanoStructured Materials, **8**, [6], 755-763 (1997).

12. S. Bhaduri, S. B. Bhaduri, and E. Zhou, "Auto Ignition Synthesis and Consolidation of Al_2O_3-ZrO_2 nano/nano Composite Powders," J. Mater. Res., **13**, [1], 156-165 (1998).

13. K. Morita, K. Hiraga , and Y. Sakka, "High Strain-Rate-Superplasticity of Y_{2O3}-Stabilized Tetragonal ZrO_2 Dispersed with 30 vol% $MgAl_2O_3$ Spinel," J. Amer. Ceram. Soc., **85**, [7], 1900-1902 (2002) .

14. M. Gust, G. Goo, J. Wolfenstine, and M. L. McCartney , "Influence of Amorphous Grain Boundary Phases on the Superplastic Behavior of 3-mole%-Yttria-Stabilized Superplastic," J. Amer. Ceram. Soc., **76**, [7], 1681-1690 (1993).

15. F. J. McKittrick and G. Kalonji, "Non-stoichiometry and Defect Structures in Rapidly Solidified MgO-Al_2O_3-ZrO_2 Ternary Eutectics," Mater. Sci. & Engin., **A231** , 90-97 (1997).

16. H. J. Kim and Y. J. Kim, "Amorphous Phase Formation of the Pseudo-binary Al_2O_3 Alloy during Plasma Spray Processing," J. Mater. Sci., **34**, 29-33 (1999).

17. A. Rosenflanz, M. Frey, B. Endres, T. Anderson, E. Richards, and C. Schardt, "Bulk Glasses and Ultrahard Nanoceramics Based on Alumina and Rare-earth Oxides," Nature, **430**, [12 August], 761-764 (2004).

18. H Keshavan, A Petersson, and W R Cannon,"Forging of Spherical Beads with Nanocrystalline Microstructures: Kinetics of Densification," unpublished work.

19. T. C. Chou and T. G. Nieh, "Nucleation and Concurrent Anomolous Grain Growth of α-Al_2O_3 During γ-α Phase Transformation," J. Amer. Ceram. Soc., **74**, [9], 2270-2279 (1991).

20. Y.-Z. Li, C. Wang, H. M. Chan, and M. P. Harmer, "Codoping of Alumina to Enhance Creep Resistance," J. Amer. Ceram. Soc., **82**, [6], 1497-1509 (1999).

21. I. W. Chen and L. A. Xue, "Development of Superplastic Structural Ceramics," J. of Amer. Ceram. Soc., **73**, [9], 2585-2609 (1990).

HOT-PRESSING AND HOT-FORGING OF POLYCRYSTALLINE POWDER PARTICLES WITH UNIQUE MICROSTRUCTURES

W. R. Cannon[1, a], A. Petersson [1, b], C. Auechalitanukul[1, c], H. Keshavan[1, d], A. Cuitino[2,e]

[1]Department of Materials Science and Engineering, Rutgers University, 607 Taylor Rd, Piscataway, NJ, USA, 08854-8065

[2] Department of Mechanical and Aerospace Engineering, Rutgers University, Brett and Bowser Rd, Piscataway, NJ, USA

[a]cannon@rci.rutgers.edu, [b]andersp@rci.rutgers.edu, [c] chira@eden.rutgers.edu, [d]hrishi@eden.rutgers.edul, [e]cuitino@jove.rutgers.edu

Keywords: hot pressing, hot forging, creep, microstructure, nanostructure.

Abstract. The kinetics of hot pressing and the resulting microstructure of two types of polycrystalline spherical powders (beads) were studied. The first were spherical ZrO_2 beads synthesized by sintering TOSOH spray dried ZrO_2 powder loose in a crucible. The average bead diameter was 51 μm and contained 0.3 μm grains. The second were Al_2O_3-ZrO_2(1%Y_2O_3) synthesized by plasma spraying spray dried powders into water to quench-in a partially amorphous, partially nanocrystalline structure. The particle size was <25μm. Densification in both cases depended on creep of the beads and densification rates at 1350ºC were predicted well both by equations from Helle et al.[1] for hot isostatic pressing and a finite element analysis method. The microstructure of the Al_2O_3-ZrO_2(1%Y_2O_3) was much more complex but densification kinetic also followed the Helle et al.[1]equations if creep data from hot pressed specimens of the same powder were substituted into the equations rather than literature values.

Introduction

Many studies have sought to improve microstructures through controlled processing and sintering. More recently a large number of studies have sought to develop nano-scale microstructures. The usual route to achieve a particular microstructure is to choose a mixture of powders, processing and sintering conditions to yield the desired microstructure. For instance, to obtain a nanostructure, the green part is formed from nano-diameter powders and an attempt is made to maintain the nano-scale through the sintering or hot pressing process. There are several disadvantages to this approach. For instance, handling of nano-powders is difficult and it is even more difficult to control the microstructure through sintering. An alternative approach [2] is to use larger diameter powder in which the microstructure is either already developed within the particle or to use an amorphous or partially amorphous powder, in which the microstructure is developed through nucleation and growth during sintering or annealing. In our studies powders were 2-55 μm in diameter and spherical so that they were easy to process. The consequence, however, is that there is too little driving force for pressureless sintering and so our studies have focused on hot pressing.

The paper will presents a model study of idealized spherical powder beads of zirconia averaging 51 μm containing submicron grains and Al_2O_3-ZrO_2(1%Y_2O_3) beads (designated as Al_2O_3-(1Y)ZrO2) with <25μm sized powder beads which are quenched from the melt and are partially amorphous and partially nanocrystalline.

For multigrain particles where the grain size is submicron or nano-sized, Nabarro-Herring, Coble, or superplastic creep controls densification under pressure since the diffusion distance for creep is much smaller than the diffusion distance for sintering, i.e. across the submicron grains vs. across the 5-51 μm particle neck. Thus instead of the pressure acting as an additional driving force for diffusion along the neck it acts as the driving force for creep. Since creep behavior is well known for many materials, densification can be modeled by considering the deformation in a single particle and then an assemblage of particles. This is much simpler than modeling of sintering processes.

Helle et al.[1] made several simplifying assumptions to earlier work [3] [4] to arrive at simple equations for densification by either power law creep or diffusional creep. For power law creep

$$\dot{\varepsilon} = B\sigma^n \tag{1}$$

where B is a temperature and grain size dependent constant and σ is stress. By combining several equations from reference [1] the densification rate, $\dot{\rho}$ in the early stage of densification, before pore closure, i.e. a relative density, $\rho \le 0.9$, may be written in terms of measurable quantities as

$$\dot{\rho} = 3.1\rho^{\frac{2}{3}}\rho_0^{\frac{1}{3}}B\left(\frac{\sigma_a}{3\rho^2}\right)^n\left(\frac{1-\rho_0}{\rho-\rho_0}\right)^{n-\frac{1}{2}} \tag{2}$$

where ρ_0 is the initial relative density and σ_a is the applied pressure, assumed in the current paper to be the uniaxial pressure. This derivation assumes that the particle coordination number, Z, varies directly with density according to the equation

$$Z = 12\rho \tag{3}$$

For instance, the relative density of our model ZrO_2 was 0.65 and so Z=7.8 initially and at full density Z=12.

In the final stage, i.e. ρ>0.9, the densification rate is given by [1]

$$\dot{\rho} = \frac{3}{2}B\left(\frac{3\sigma_a}{2n}\right)^n \frac{\rho(1-\rho)}{\left[1-(1-\rho)^{\frac{1}{n}}\right]^n} \tag{4}$$

Neither of these equations contains particle size dependence but only grain size dependence. In a previous paper[5] it was shown that experimentally there is only a slight dependence of particle size Therefore, to the first approximation, particle size and shape may be chosen for the convenience of manufacturability.

The value of B and n may be supplied from literature creep data to predict the densification rate up to full density. For the case of ZrO_2, [6] Jiménez-Melendo et al. provide the creep equation for Y-ZrO_2 from a compilation of creep literature results (creep is insensitive to Y_2O_3 content)

$$\dot{\varepsilon} = \frac{B' \exp\left(-Q/RT\right)}{Td^2}\left(\sigma - \sigma_0\right)^2$$

(5)

Where B' is a constant , Q is the activation energy, σ_0 is the threshold stress, and d is the grain size. Thus Eq. (2) becomes

$$\dot{\rho} = 3.1\rho^{\frac{2}{3}}\rho_0^{\frac{1}{3}}\frac{B' \exp\left(\frac{-Q}{RT}\right)}{Td^2}\left(\frac{\sigma_a - \sigma_0}{3\rho^2}\right)^2\left(\frac{1-\rho_0}{\rho-\rho_0}\right)^{\frac{3}{2}}$$

(6)

and Eq. (4) becomes

$$\dot{\rho} = \frac{3}{2}B'\frac{\exp\left(\frac{-Q}{RT}\right)}{Td^2}\left(\frac{3\left(\sigma_a - \sigma_0\right)}{2n}\right)^n \frac{\rho\left(1-\rho\right)}{\left[1-\left(1-\rho\right)^{\frac{1}{n}}\right]^n}$$

(7)

Though creep literature is available for many other potential compounds, the microstructure of the quenched bead under hot pressing conditions do not have such easily characterized microstructures [2] and it may be difficult to take values of B' and n directly from the literature. The approach taken in this paper was to hot press samples to a point where creep can be measured and then remove them from the die and measure the creep rate correcting it for porosity using the Langdon correction. [7]

In this paper experimental hot pressing rates of the model ZrO_2 and of quenched Al_2O_3-(1Y)ZrO_2 beads mentioned above will be compared with rates from Eqs.(2), (4), (6) and (7) and with a finite element model.

Only a few studies have specifically mentioned hot pressing of polycrystalline powders. For instance, Bhaduri et al. [8] synthesized by an auto ignition technique Al_2O_3-10% ZrO_2 particles which contained nanocrystalline microstructures and then hot isostatic pressed compacts at 1200°C. Zhou et al. [9] have synthesized beads in a similar manner to this study but have subsequently ground them to fine powder and sintered them by the spark plasma method. McEnerney et al. also synthesized beads in this manner and ground them to fine powder then HIPped them to full density.[10] None of these studies, however, discuss kinetics of densification by creep.

Experimental

ZrO_2 Sintered Powder. Spherical multigrain zirconia (0.25mass% Al_2O_3) beads were prepared by sintering commercial spray-dried granules (TZ-3Y-E, Tosoh Corporation, Japan) loose in a crucible at 1400ºC for 2 hours. To break apart bridges between granules, after sintering, powder was ball milled for 24 hours with zirconia grinding media. The beads maintained their spherical shape with very few fragmented particles while eliminating bridges between beads. The beads was then screened to eliminate

beads <45 μm and less than >53 μm. The mean bead diameter after screening was 51 μm and the mean grain size of the as-sintered particles was 0.3 μm. Grain size was measured on the surface of the particles which was sufficiently thermally etched to see grain boundaries. The average grain diameter, $d_{avg.}$ was calculated from the average line intercept length l_{avg} according to the equation

$$d_{avg} = 1.56 l_{avg}$$

(8)

Powder was hot pressed in a SiC (Hexaloy, Saint Gobain, Niagra Falls, NY) die (7.3 mm ID) in air at 1350ºC in a creep rig equipped with an extensometer to measure the deformation continually. The high thermal expansion coefficient of ZrO_2 and Al2O3-(1Y)ZrO2 allowed release of the specimen upon cooling and the dies were soaked in dilute HF to dissolve away silica. Before pressing, the powder was poured into the die, placed on top of a vibrating table, and allowed to settle for several to achieve the maximum packing density. The packing density of the ZrO_2 was 65% of theoretical. This is higher than the theoretical random packing density of 62% for monodisperse particles because of the wider particle size distribution. The packing density was, therefore, sufficiently high that initial particle rearrangement during hot pressing is believed to be insignificant. Hot pressing was performed in a compression creep rig (ATS, Butler, PA).

Al_2O_3 –ZrO_2 Melt-Quenched Powder. Spherical multigrain powders were fabricated by first spray drying a eutectic (67vol.% Al_2O_3-33 vol.% ZrO_2) mixture of Al_2O_3 (Almatis, A16SG, Bauxite AR) and ZrO_2 (Magnesium Electron Inc., Manchester, England)-1% Y_2O_3. (Unocal Molycorp, Mountain Pass, CA). Spray dried aggregates were calcined at 1000ºC for 4 h to eliminate binder and impart strength to the aggregates. The spray dried granules were then plasma sprayed into a water bath resulting in a quenching rate of ~10^4 ºC/s. [2] As a result of rapid quenching the powders were about ~30-40% amorphous and the rest contained crystallites between 20 and 50 nm in diameter. Almost all beads <25μm in diameter viewed under an optical microscope were fully transparent. Some of the larger sized beads were not fully melted. Thus the powder was sieved to retain powder <25 μm for hot pressing.

Powder was pressed in a SiC die. The green density was approximately 64% of theoretical density based on the He-pycnometer density of the as-quenched beads of 4.1 g/cm^3. The slightly lower green density for the as-quenched beads is probably related to the more uniform size distribution of these beads. Creep testing was performed in a universal testing machine (Instron with an electromechanical actuator) under constant load while the rate of the cross head was monitored. The final length agreed with the crosshead movement within 5%.

To obtain creep results for the eutectic Al_2O_3-(1Y)ZrO_2, beads were pressed in a die fabricated from commercial alumina tubes (4.6 mm ID) with commercial alumina rods to fit tight in the tube and cut to a short length. Sufficient powder was added to make the final length of the pressed pellet ~4 mm. The powders were only hot pressed in the die sufficiently long to give the pellets sufficient strength to be removed by breaking the die. They were then further densified by forging without radial constraint. The axial strain rate determined after one hour when the density was ~85% of theoretical was corrected for the effect of porosity to yield the creep rate needed for Eq. (2). In this way the creep

rate was determined in approximately the same microstructural state as it is in the hot pressing experiment.

Finite Element Studies

Finite element analysis was used to calculate the densification rate in order to compare with predictions of Eqs. (2), (4), (6) and (7). The code determines the distribution of elastic stresses within a 3-D spherical particle under diametrical z axis loading with lateral confinement after a displacement, *dz*. Then it allows each element to creep for a time period, *dt* and then the stresses are recalculated. The sequence is repeated in order to obtain a stress-density curve. An example of the stress distribution within a quadrant is shown in Fig. 1 at two different stages of densification.

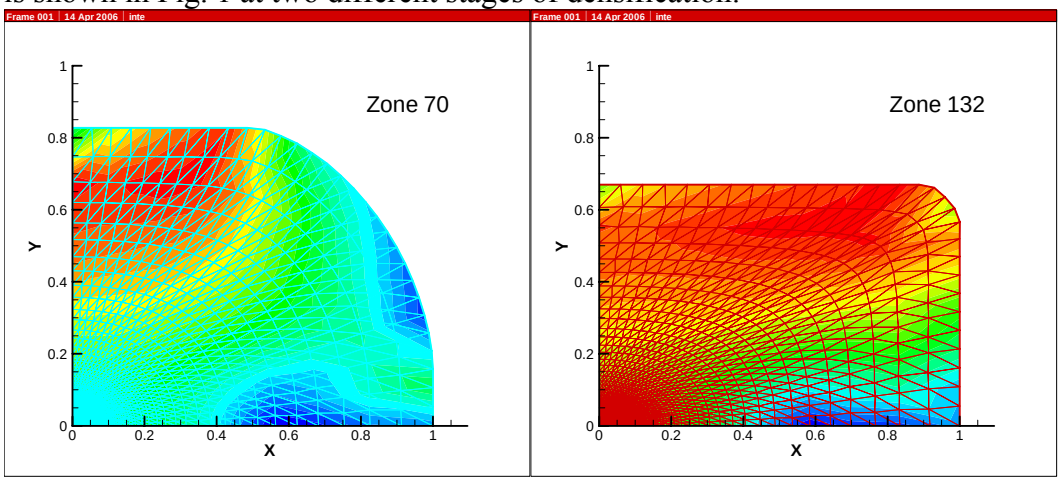

Figure 1. Finite element stress distribution of the upper right quadrant of a diametrical slice at two different stages of densification by creep.

A series of stress-density curves are generated at different displacement rates. The density at the same pressure was picked from every curve and then the densification rate vs. density was plotted for a pressure of interest. This analysis, therefore, assumed that the strain rate is independent of the load strain rate history.

Results

Fig. 2(a) compares $\dot{\rho}$ vs.ρ experimental results for ZrO_2 with values calculated from Eqs. (6) and (7) at 1350ºC and 40 MPa and Fig. 2(b) compares the experimental values for quenched Al_2O_3-(1Y)ZrO_2 beads with predictions from Eq. (2), both at 1350ºC and 40 MPa. The following values were used in Eqs. (6) and (7) and for FEM calculations for ZrO_2, n=2 $B' = 4x10^{10}\,\mu m^2 KMPa^{-2}s^{-1}$, $\rho_o = 0.66$ $\sigma_o = 1MPa$, Q=461 kJ/mol, and d=

0.3 μm [11]. In the present experiments TZ-3Y-E ZrO_2 requires using creep data for Al_2O_3 doped ZrO_2. [11] For the quenched Al_2O_3-(1Y)ZrO2 Eqs. (2) was used. Since values were taken directly from our creep experiments on these materials at 1350ºC, it was not necessary to know the grain size or activation energy. The values taken from creep experiments were n=1.2, $\rho_o = 0.66$ and $B = 4x10^{-8}$ MPa^{-2}s^{-1}. In both cases the stress was 40 MPa and temperature 1350ºC. Densification rates of Al_2O_3-(1Y)ZrO_2 were sufficiently slow that only 75% density was achieved in one hour.

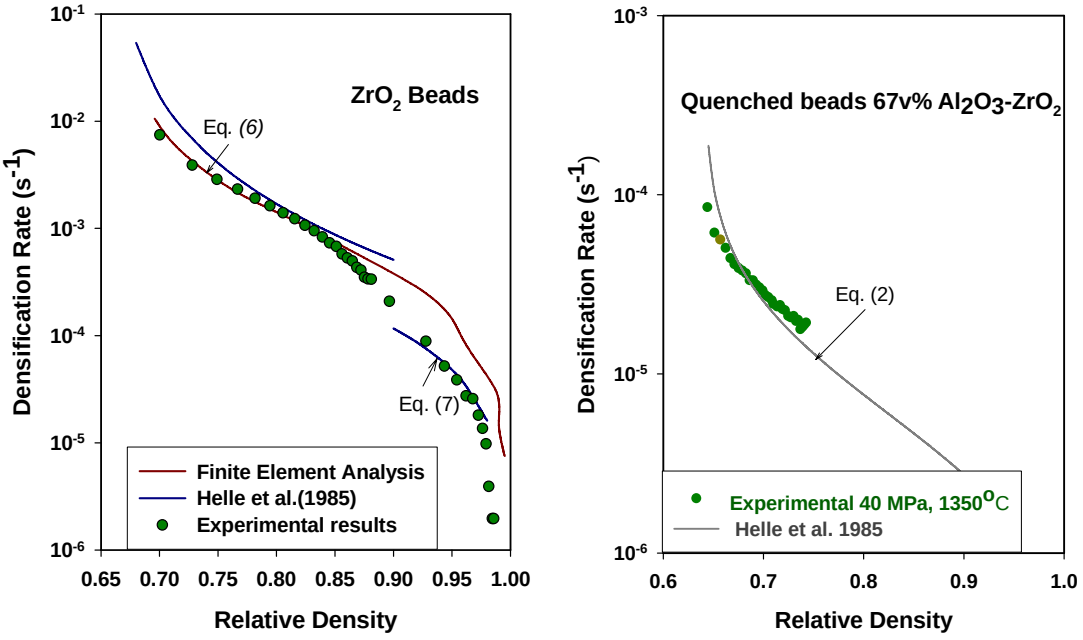

(a) (b)

Figure 2. A comparison between experimental with Eqs. (2) (6) and (7) and with the FEM calculations at 1350ºC and 40 MPa for (a) ZrO_2 and (b) Al_2O_3-(1Y)ZrO_2 beads.

Both the FEM and Helle et al.[1] predictions fit the experimental values for ZrO_2 and Al_2O_3-(1Y)ZrO_2 extremely well. This is surprising considering the predictions are based on creep results which often vary by a factor of two or three between investigators. Jimenez-Melendo et al.'s [6] compilation of creep literature, for instance, indicates an approximate order of magnitude variation in creep rates between investigators and is dependent on purity

An expected source of difference between the experimental and predictions of Eqs. (2), (6) and (7) is that experiments were conducted by uniaxial pressing in a die whereas the predictions were for isostatic pressure. On the other hand, the FEM simulations assumed uniaxial pressing with lateral confinement. Neither considers die-wall friction, which would effectively reduce the pressure.

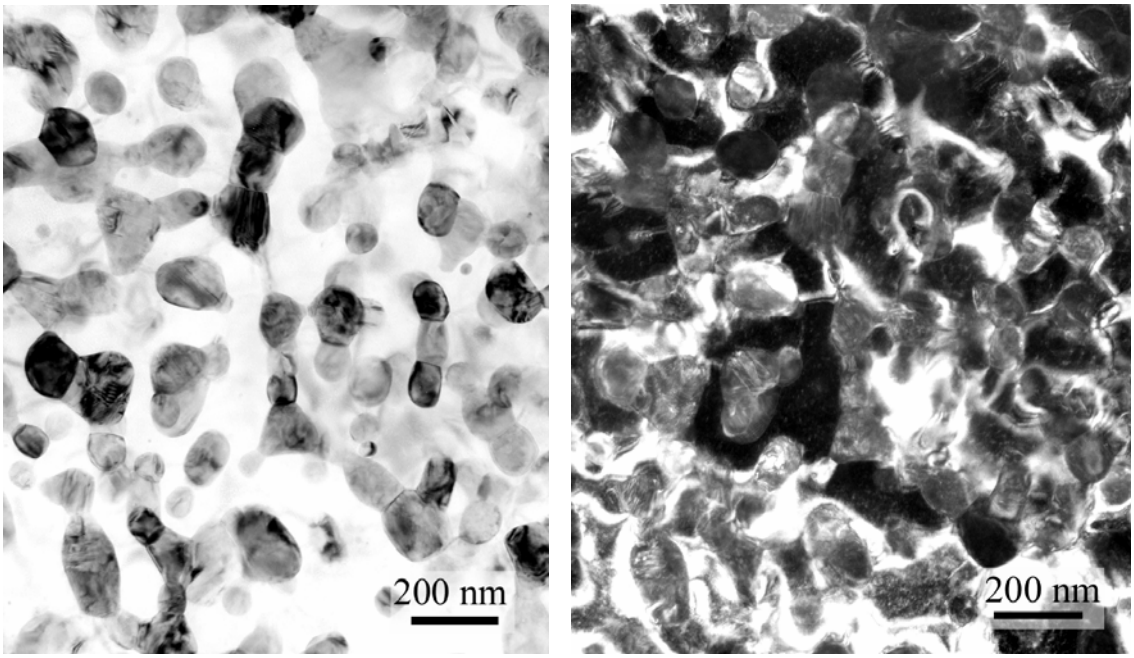

(a) (b)

Figure 3. TEM micrographs of quenched 67vol.% Al_2O_3-ZrO_2 after forging at 1350ºC. (a) ZrO_2 is dark and Al_2O_3 is light in bright field. (b) In dark field the brightest portions come from one Al_2O_3 diffraction spot. The aperture may also have covered a ZrO_2 spot.

In analyzing the hot pressing of quenched Al_2O_3-(1Y)ZrO_2 beads, it is quite difficult to use literature creep values since the microstructure is rather complex and it is difficult to determine the appropriate grain size. A detailed description of the microstructure of the beads hot pressed at 1350ºC is contained in a future paper. The microstructure is not uniform throughout but some simplified observations may be made. Briefly, Al_2O_3 forms the continuous phase with ~100 nm diameter ZrO_2 particles imbedded in the Al_2O_3 matrix as shown in Fig.3(a). Selected area diffraction (SAD) pattern indicates a polycrystalline nature to ZrO_2 and Al_2O_3 but in the Al_2O_3 rings very few spots are present indicating that crystallites may be on the order of the aperture size which is less than one micron. There are also some regions of the microstructure where single crystalline SAD patterns are observed. The morphology and size of the Al_2O_3 crystallites can better be determined from the dark field image shown in Fig 3(b). The image was taken from a diffraction spot in an Al_2O_3 ring. It appears that some of the Al_2O_3 is of a single orientation extending continuously behind the ZrO_2 particles. Other Al_2O_3 has a different orientation. Even though the crystallite dimension extend for more than one micron, portions of the Al_2O_3 matrix have another orientation since they show up as very dark. We conclude that there is an

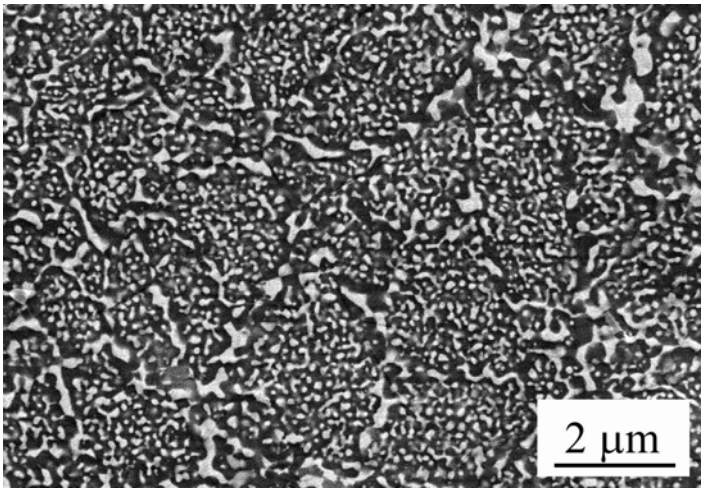

Figure 4. SEM micrograph of Al_2O_3-(1Y)ZrO_2 forged at 1350 ^oC for 1 h at ~50 MPa. Al_2O_3 is dark phase and ZrO_2 is light phase.

intertwining of Al_2O_3 matrix grains. This is consistent with the ring SAD pattern, which showed more than one diffraction spot in these areas.

At lower magnifications a second feature is observed. Cell boundaries appear, which are decorated with ZrO_2 stringers as shown in Fig. 4. The mean size of these features is approximately 2 μm. It is uncertain whether these coarser features are compositional remnants from the melt quench or whether they are related to the growth of α-Al_2O_3 from γ or δ-Al_2O_3. The discussion below attempts to decide whether the finer features or the coarser features are the creep controlling ones. The roll of grain boundaries in diffusional or superplastic creep is that they must either be a source and sink of vacancies or a source of grain boundary sliding.

Models which best fit creep of two phase ceramics [12], [13] indicate that the most creep resistant phase, especially if it is the most abundant, dominates the creep rate of the composite. In this case Al_2O_3 should dominate the creep resistance. Thus to a first approximation the grain size of the Al_2O_3 phase should be the dominant feature of the microstructure that determines creep rates. Fig. 5 takes literature values [14]for creep of Al_2O_3-(1Y)ZrO_2 of approximately the same composition (69%Al_2O_3·31%(ZrO_2 -3 %Y_2O_3)) to substitute into Eqs. (6) and (7). In this case we have fit to several different Al_2O_3 grain sizes not knowing the exact grain size. The shape of the curve is strongly affected by the stress exponent, n and so two different stress exponents were used, the one we obtained from our creep studies on these materials and the other from the literature value from Wakai et al. [14] Although none seem to fit well, 1-2μm size range appear to be a reasonable size.

Discussion of Results

The Helle et al. [1] equations are simple to use and accurately predict densification in this study, but so do the finite element prediction. Each has their strength. The Helle et al. equations more properly handle the particle coordination throughout densification as compared to the finite element predictions. The finite element predictions assume radial confinement and uniaxial pressure throughout densification, which is most closely approximated with 6-fold coordination. On the other hand, the finite element approximation considers the

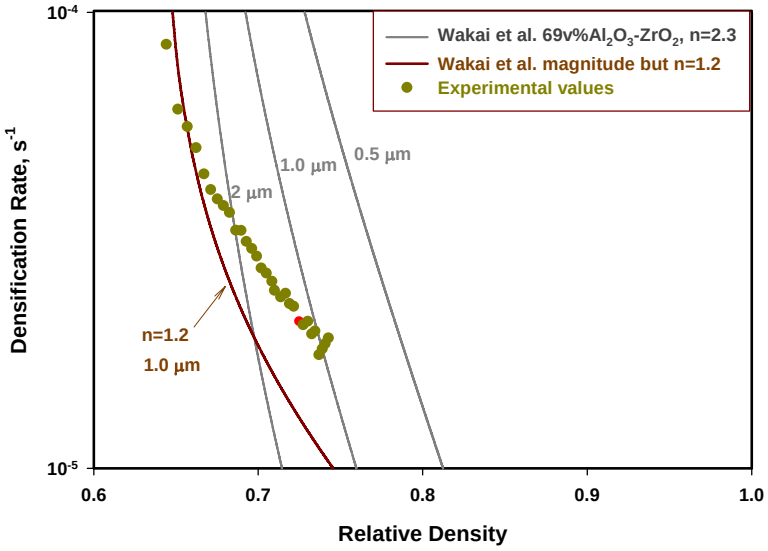

Figure 5. Predicted densification rates using Eqs. (6) and (7) substituting creep results from Wakai et al.[14] compared to experimental rates. Both n=1.2 from the present creep results and n=2.3 from Wakai et al.[14] were used.

stress distribution in the particle, whereas the Helle et al. equations merely take an average force applied to a particle divided by the contact area.
Another issue is that the Helle et al. equations base densification rates on and applied isostatic pressure, where as the finite element calculations consider uniaxial pressure with laterial confinement as expected for hot pressing. The particular finite element model we used predicts no laterial stress on the particles in the early stage of densification but the stress becomes more isostatic as densification proceeds. This would mean that the Helle et al. model overestimate the densification rate in the early stages. However, the finite element model applies the force directly to the polar cap of the sphere along the z axis. In reality particles apply a force at an angle to the z axis and, therefore, exert some lateral force on the particle and so have some isostatic nature. Although each makes some unrealistic approximations, both seem to fit the experimental results remarkably well.

Die wall friction is potentially quite large as the particles either react, diffusion bond or mechanically grip the die wall. The first two are probably minimal between the SiC wall and either ZrO_2 or Al_2O_3-(1Y)ZrO_2 at 1350ºC. Because the creep resistance of the SiC is much greater than either ZrO_2 or Al_2O_3-$YZrO_2$, the wall remains smooth and there may be minimal mechanical gripping to the die walls. In other experiments we found that densification rates were approximately a factor of two slower when pressed in alumina die.

Finally, in making large parts where binder burnout is difficult it would appear that there is considerable advantage in first sintering the particles spray dried agglomerates of powder before hot pressing. In another paper, [15] however, it was shown that the hot pressing densification rates of the spray dried TOSOH powder as-received was faster than the sintered spay-dried agglomerates studied here. This is likely because the ultimate particle size of the commercial powder is on the order of 50 nm as compared to the 300 nm grain size of the sintered particles.

Most oxide ceramics can be spray dried and then plasma or flame sprayed into water to produce large spherical either nanocrystalline microstructure or amorphous powders. This is a convenient route to nanostructured ceramics but full control of the microstructure has not been achieved here. One particularly promising process is to choose composition which quench to the fully amorphous state. Rosenflanz et al. [16] found that the addition of rare earth oxides to Al_2O_3 or Al_2O_3-ZrO_2 lead to amorphous powder which can be pressed to full density in the amorphous state at temperatures around 920ºC. We have synthesized similar powders and find that their viscosity at ~920ºC is as low as Al_2O_3-(1Y)ZrO_2 at 1350ºC

Summary

The densification behavior of two types of spherical, micron-sized polycrystalline powders (beads) was studied. The first was fabricated merely by sintering commercial spray dried 3$YZrO_2$ loose in a crucible. The other was quenching from a melt spray dried Al_2O_3-3$YZrO_2$. In the first case the spherical particles were dense and contained a well defined microstructure with grains 0.3 μm in diameter. In the second the microstructure was partially amorphous and developed a microstructure which was rather complex. Measured densification rates can be predicted with the equations of Helle et al.[1] intended for hot isostatic pressing and from a finite element method. Both predictions for

the ZrO_2 hot pressing were excellent and agreed well with each other. These predictions also fit the Al_2O_3-(1Y)ZrO_2 when creep data creep data from the same material was used but approximately when literature values were used. In the latter case was difficult to decide what grain size data to substitute into the equations.

Acknowledgement

Financial support for this work came from Basic Energy Sciences Division of the Department of Energy Grant Number DE-FG02-O2ER46010.

References

1. A.S.Helle, K.E.Easterling, and M.F.Ashby, Acta Metall, Vol.33, (1985) p.2163.

2. S.Balasubramanian, H.Keshavan, and W.R.Cannon, J. Eur. Ceram. Soc., Vol.26, (2005) p.1359.

3. H.F.Fischmeister and E.Arzt, Powder Metall., Vol.26, (1983) p.82.

4. E.Arzt, M.F.Ashby, and K.E.Easterling, Metall. Trans. A, Vol.14A, (1983) p.211-221.

5. Auechalitanukul, C, Cuitino, A, and Cannon, W R, Proceedings of the 107th Annual Ceramic Society Meeting(2005)

6. M.Jimenez-Melendo, A.Dominguez-Rodriguez, and A.Bravo-Leon, J. Amer. Ceram. Soc., Vol.81, (1998) p.2761.

7. T.G.Langdon, J. Amer. Ceram. Soc., Vol.55, (1972) p.630.

8. S.Bhaduri, S.B.Bhaduri, and E.Zhou, J. Mater. Res., Vol.13, (1998) p.156.

9. X.Zhou, D.M.Hulbert, J.D.Kuntz, K.Sadangi, V.Shukla, B.H.Kear, and A.K.Mukherjee, Mater. Sci. Eng. A, Vol.394, (2005) p.353.

10. B.W.McEnerney, G.D.Quinn, V.A.Greenhut, K.Sadangi, V.Shukla, B.H.Kear, and D.E.Niesz, Ceram. Sci. Eng. Proc., Vol.25, (2004) p.647.

11. E.Sato, H.Morioka, K.Kuribayashi, and Sundararaman D., J. Mater. Sci., Vol.34, (1999) p.4511.

12. J.D.French, Y.Zhao, M.P.Harmer, H.M.Chan, and G.A.Miller, J. Amer. Ceram. Soc., Vol.77, (1994) p.2857.

13. L.Clarisse, R.Baddi, A.Bataille, J.Crampon, R.Duclos, and J.Vicens, Acta Mater., Vol.45, (1997) p.3843.

14. Wakai, F, Kodama, Y, Sakaguchi, S, Murayama, N, Kato, H, and Nagano, T, MRS Intl. Meeting on Advanced Materials, Vol.7, (1989) p.259.

15. Auechalitanukul, C. and Cannon, W R, Ceramic Transactions, In Press

16. A.Rosenflanz, M.Frey, B.Endres, T.Anderson, E.Richards, and C.Schardt, Nature, Vol.430, (2004) p.761.